Characterization of Conditioned Nuclear Waste for its Safe Disposal in Europe

CHANCE project

(Contract Number: 755371)

PERFORMANCE OF THE MUON TOMOGRAPHY DETECTOR SYSTEM
DELIVERABLE (D4.1)
Work Package 4

Author(s): **J. Velthuis, D. Barker, C. De Sio, D. Kikola, A. Kopp, P. Stowell, L. Thompson**

Reporting period 3: 01/06/2020 – 31/03/2022

Date of issue of this report: **20/4/22**

Start date of project: **01/06/2017**

Duration: 58 Months

This project has received funding from the Euratom research and training programme 2014-2018 under grant agreement No 755371;		
Dissemination Level		
PU	Public	X
CO	Confidential, only for partners of the CHANCE project and EC	

History chart			
Status	**Type of revision**	**Partner**	**Date**
Draft	Initial version	UNIVBRIS, WUT and USFD	

Reviewed by
Andra

Approved by
The Executive Board

1. Introduction

The CHANCE project aims to address the specific issue of the characterization of conditioned radioactive waste. The characterization of fully or partly conditioned radioactive waste is a specific issue because unlike for raw waste, its characterization is more complex and therefore requires more advanced non-destructive techniques and methodologies.
The objective of CHANCE is to further develop, test and validate techniques already identified that will improve the characterization of conditioned radioactive waste, namely those that cannot easily be dealt with using conventional methods. Specifically, the work on conditioned radioactive waste characterization technology will focus on:

- Calorimetry as an innovative non-destructive technique to reduce uncertainties on the inventory of radionuclides;
- Muon Tomography to address the specific issue of non-destructive control of the content of large volume nuclear waste;
- Cavity Ring-Down Spectroscopy (CRDS) as an innovative technique to characterize outgassing of radioactive waste.

In the framework of work package 4, a mobile muon tomography system using RPCs and drift chambers was built and operated in a non-laboratory environment. This report details the performance and challenges in the realisation of the system.

1.1 Muon tomography

Muon scattering tomography (MST) is a noninvasive method which shows a great potential to produce 3D images of closed objects from a safe distance. MST uses cosmic rays as probes. Cosmic rays are high energy, charged particles which come to the Earth's atmosphere from outer space. In the atmosphere, cascades of new particles are produced. The main type of particles that reach sea level are muons. Muons are identical to electrons, but 200 times heavier. Muons can go through large amounts of material as they do not scatter very much due to their high mass. When traversing material, Coulomb interactions take place between the muons and the nuclei of the material. As a result, muons exit the material under an angle. The angular distribution of scattering of muons can be described by a Gaussian distribution with a mean of zero and a standard deviation σ_θ described by [1]:

$$\sigma_\theta = \frac{13.6\,MeV}{pc\beta}\sqrt{\frac{T}{X_0}}\left[1 + 0.038 ln\left(\frac{T}{X_0}\right)\right] \tag{1.1}$$

$$X_0 \approx \frac{716.4A}{Z(Z+1)ln\left(\frac{287}{\sqrt{Z}}\right)}\ [g \cdot cm^{-2}] \tag{1.2}$$

Where p is the muon's momentum, β the muon's speed divided by the speed of light c, T is the thickness of the material and X_0 its radiation length. A is the atomic weight of the medium in g·mol^{-1}. The standard deviation depends on the atomic number, Z, of the traversed material. Under the assumption that scattering occurs in single locations and by reconstructing the incoming and outgoing trajectories of the muons, the scattering angle distribution can be reconstructed and thus information about the traversed material can be extracted.

There are two ways to utilize muons: one is to record the number muons absorbed in the material, which is known as radiography, and to measure the scattering, which is known as muon tomography. The radiography is particularly relevant for the scanning of large objects like waste silos, while tomography is utilized for objects like waste drums up to cargo containers.

Muon tomography requires both the incoming and outgoing muon trajectory to be measured. Hence, the object under inspection needs to be covered on both sides. As muon tomography relies on reconstruction of the scattering angle, the key parameter for the detector system is the angular resolution of the upper and lower detector system. As such, a poor hit position resolution can be compensated for by increasing the distance between the measurement planes. That typically requires large area detectors. Due to cost reasons, these detector systems are either gaseous [2, 3][1] or scintillation detectors like for example [4]. Several types of gaseous detectors are in use: resistive plate chambers (RPC), drift chambers and drift tubes are the most common. There are two types of scintillator-based detectors in common use. All aforementioned technologies provide large area detector systems with good performance for reasonable cost.

1.2 Detector description

In CHANCE it was chosen to produce a system based on both Resistive Plate Chambers (RPCs) and Drift Chambers. The design is shown in figure 1.1. There is a lot of expertise on RPCs and drift chambers at both the University of Bristol and the University of Sheffield, see for example [5, 6, 7].

[1] [3] is an output of the CHANCE project and can be found at the end of this report as well.

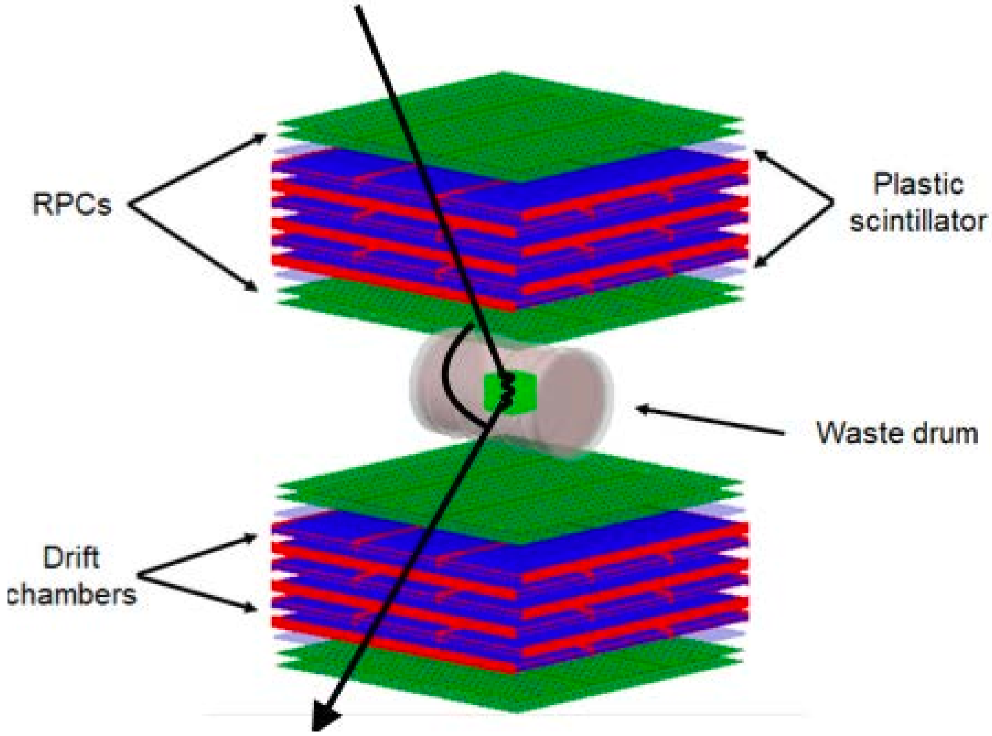

Figure 1.1. The design of CHANCE MST detector with an example of a muon showing the angle between the incoming and outgoing direction.

The system consists of 30 Resistive Plate Chambers (RPCs), see chapter 3 for details, 18 Drift Chambers, see chapter 4 for details and trigger panels, see chapter 2 for details. The panels are located in two perpendicular orientations, namely X and Y: each orientation detects hits in the (X, Z) and (Y,Z) planes, respectively, together forming a 3D track. It was chosen to operate the detector in a non-laboratory environment. The detector, see figure 1.2, is hosted at the Fenswood Farm, 5 miles south-west of Bristol, UK.

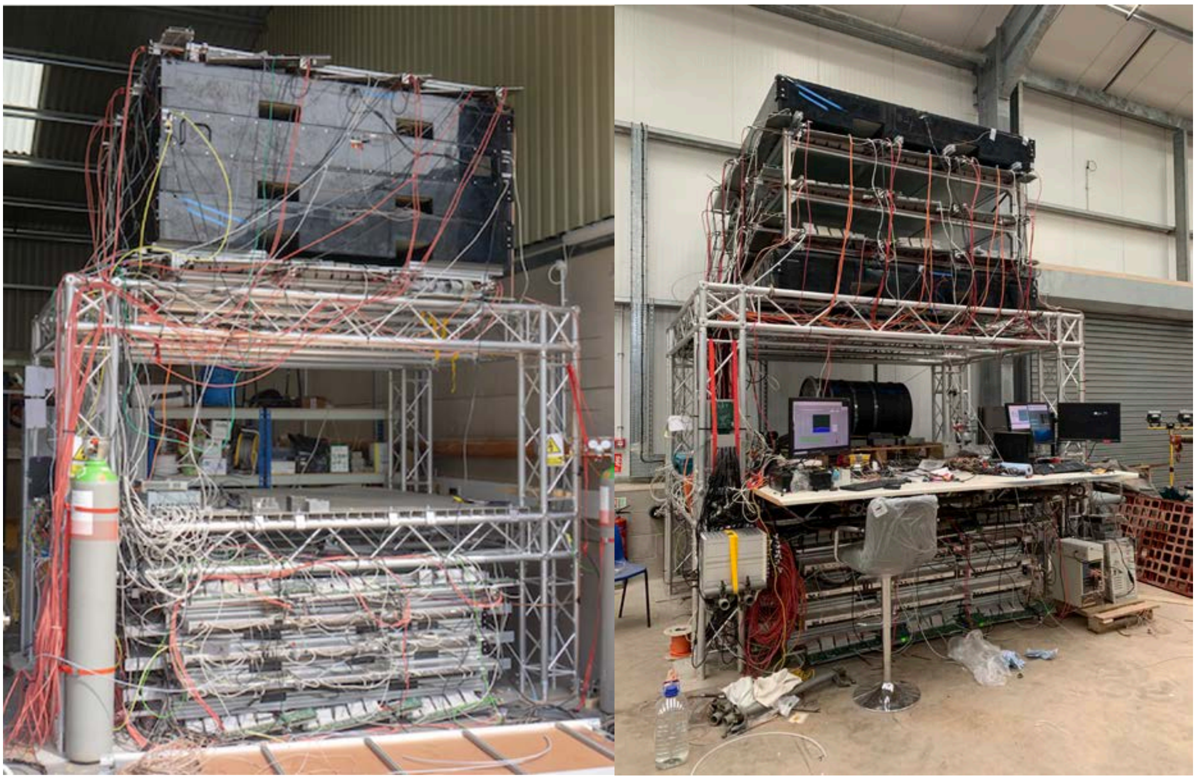

Figure 1.2: The CHANCE detector at Fenswood Farm in the first barn (left) and the second barn (right).

2. Trigger system

Both of the tracking subsystems of the CHANCE detector require an external trigger to know when the muon crossed through the detector and initiate a readout cycle. This is especially important for the drift chamber subsystem as it is used in time of arrival calculations.

2.1 Trigger Paddles

To provide an external trigger to the CHANCE subsystems, two scintillator trigger paddles are used. As shown in figure 2.1, they comprise of 300 20 cm × 20 cm injection moulded plastic scintillator tiles arranged to form a 200 × 200 cm scintillating trigger paddle. Each of the individual tiles is embedded with 4 wavelength shifting fibres (120 fibres total per paddle), with fibres from all tiles being grouped together and coupled to a single ET Enterprises 9902B photomultiplier tube. These PMTs are powered by a ET-HV3820AN base, which requires only a 5V power supply and a 0-1.3V control voltage input. The control voltage for the PMT HV is provided by an ADAM 4024 analogue control unit, to provide a network accessible and temperature stable slow control for the trigger paddles. The HV is typically operated at a control voltage of 1.28V, corresponding to 1280V on the PMT power supply.

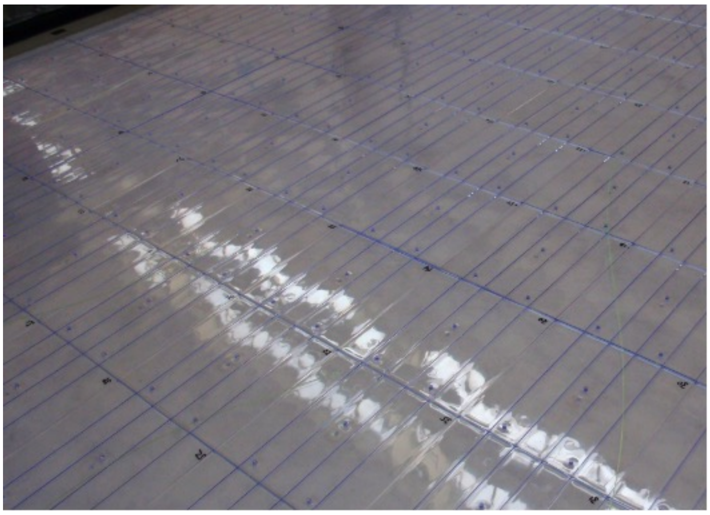

Figure 2.1: Single scintillator trigger paddle consisting of layers of scintillating tiles readout with wavelength shifting fibres.

2.2 Coincidence Detection

To provide a reliable trigger for muons that have passed through the muon tracking subsystems, and reject background noise, a coincidence discriminator unit is required to ensure that both scintillator paddles are triggered within a short timing window. This coincidence discriminator is provided by a small discrimination unit developed by the University of Bristol. The input and output schematics of this board are shown in figure 2.2. During normal operation the unit takes the input signals from the scintillator paddles, and passes each one through a fixed threshold discriminator (ADCMP604) to produce a digital pulse for interpretation by an FPGA. The threshold for this discriminator stage is adjustable by a manual POT for each channel. Coincidence triggering logic between both inputs is handled internally on a CMOD A7 FPGA, before an external trigger signal is issued to each of the separate tracking subsystems. In addition to this basic coincidence logic, busy signals are provided by the RPC and drift subsystems so that no trigger signals are issued whilst either subsystem is busy, helping to synchronise the trigger event indices between the two subsystems.

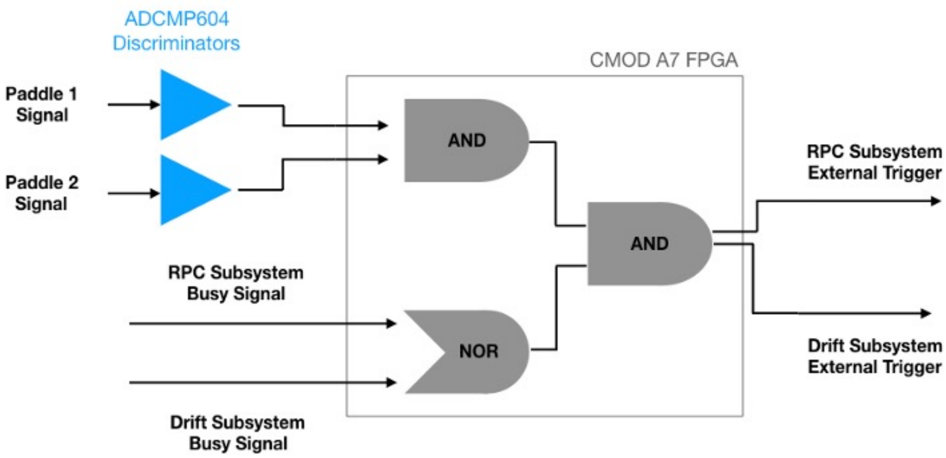

Figure 2.2: Coincidence discriminator board logic used to issue external trigger signals to the RPC and Drift Chamber subsystems.

2.3 Coincidence Rate

The coincidence detection rate for the system is approximately 40 Hz during normal operation. Compared to normal operation this corresponds to roughly 30% of the total muons passing through the system. It is expected that this could be improved by replacing the manual potentiometers on each of the discriminator stages with digital ones. This would allow precise optimisation of the thresholds for the trigger system with minimal user input, however 40 Hz is a sufficiently large trigger rate that useful tracking data can be obtained from each of the CHANCE subsystems.

3. RPC system

An RPC essentially consists of a chamber filled with gas under a high voltage (HV). When a charged particle traverses the gap chamber, ionisation takes place. Under the influence of the high voltage, a current pulse is produced. This induces a signal on pick up strips on the outside of the sensor. These signals are read out to detect the particle and reconstruct where it traversed the detector. An image of a single RPC is shown in figure 3.1.

The large chambers were manufactured by an external glass company and tested in our laboratories to ensure that they all passed minimum quality criteria. The top and bottom surfaces of the RPCs are coated with conductive paint, Statguard Conductive Acrylic Paint, to create a thin film with surface resistivity of $10^5\Omega/m^2$. The film is used to create a uniform electric field within the gas cavity by applying HV to it. Two sheets of 1 mm thick PETG are glued to the RPCs to insulate the HV planes. Each RPC is mounted on an aluminium tray to increase its mechanical rigidity. The trays are designed to be slid in position on a larger mechanical support and to host the front-end electronic boards. A layer of RPCs as used in the CHANCE system is shown in figure 3.2.

Figure 3.1: Exploded view of an RPC (left) and an assembled RPC (right)

A single PCB with 1.68 mm pitch readout strips is glued on the top of each RPC. 320 strips run along the length of the PCB and are read out by a single board [8], designed in Bristol, which digitizes their signal and transmits them to the DAQ. Each board hosts five MAROC readout chips [9], each one connected to 64 strips. When a trigger signal is received, see chapter 2, the inputs are digitized using the 12-bitWilkinsons converters built in each MAROC and the samples are stored in a buffer to be read by the DAQ system. The trigger signals are distributed via HDMI. The communication between DAQ and front-end boards is based on the IPBus protocol [10] and is performed using a standard giga-Ethernet connection. The RPC data acquisition software is written in Labview[11]. It reads the data from each RPC and stores it in a binary format. The RPC panels are powered by a high voltage power supply, applying a maximum of ±5kV to each side. Each readout board is powered by a dedicated low voltage power supply. For each trigger the RPCs are read out, the signals of all strips stored and the data is analysed off-line.

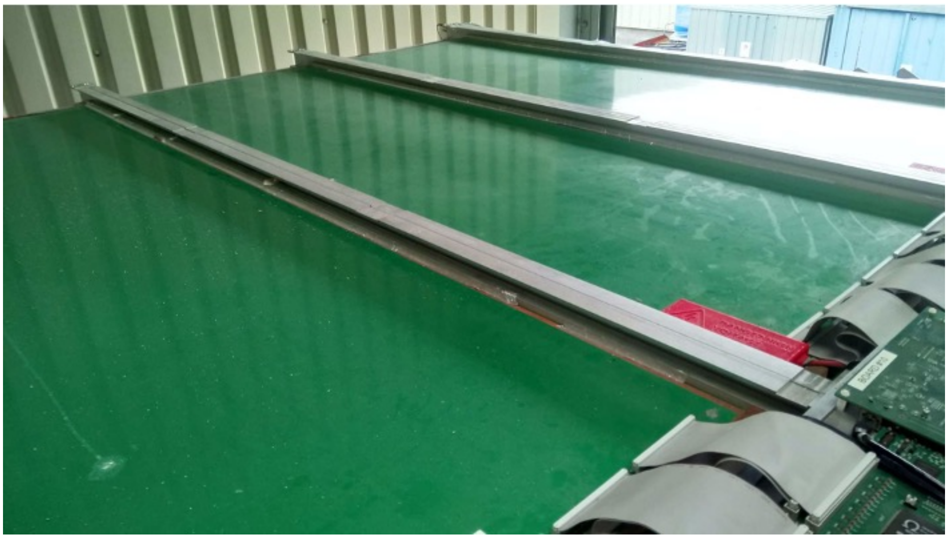
Figure 3.2: An RPC layer inside the CHANCE system.

3.1 RPC drift gas

These systems have achieved spatial resolutions better than 500 mm and efficiency above 95% when flushed at a rate of 25 ml/min with a mixture of Tetrafluoroethane R-134a (95%) and Iso-butane (5%) at a pressure of about 500 Pa (2 inches of water) above the atmospheric pressure [5]. R-134a is a very good gas for RPCs. In R-134a on average 81.6 electron-ion pairs are produced per mm as primary ionisation [12]. The primary electrons then undergo multiplication processes to generate the signal. Unfortunately, R-134a is very bad for global warming. Due to stricter environmental regulations coming into force during the CHANCE project, we were forbidden from using R-134a. It became impossible to buy R-134a in the UK without a special permit, which we did not get. To keep using R-134a would required the installation of an abatement system. We requested an informal quote for such a system, which was around £200,000. We did not have the budget to buy such a system. In addition, it would have required significant works on site and it was not clear we would be able/allowed to install such a system.

As we could no longer use R-134a, it was decided to switch to CO_2 instead. CO_2 only has an average of 35.5 electron-ion pairs are produced per mm as primary ionisation and 91 electron-ion pairs are produced per mm in total [13]. There are many RPC systems that successfully operate with CO_2. As such the signal in the CO_2 filled RPCs is much lower (around 5–10 times) than expected when designing the system, which lowers the hit efficiency dramatically. To get a good efficiency with CO_2 requires a combination of either a thicker gap, so more total ionisation takes place, and/or a larger electric field and thus a much higher high voltage. This problem is not unique to us. Many groups and systems operated around the world have encountered the same problems. There is a lot of work being done trying to find environmentally friendly and affordable alternatives, see for example [12, 14, 15, 16], but they are not (yet) available at a price and bottle size that made using it viable. As a result, we had to decide to increase the RPC voltage as much as we could and accept the lower efficiency in the hope that a better alternative became available soon.

3.2 RPC data

When a coincidence trigger arrives, RPC events are written to disk. For each RPC in each event the data is composed of a header, which contains the IP address identifying the readout board, the trigger number identifying the event, the recorded timestamps and the ADC signals of all strips, see figure 3.3. The data are subsequently processed as described in section 3.3. An example of a fully processed event in a single RPC is shown in figure 3.4.

BINARY

0) IP ADDRESS - 1 word
1) TRG # TS - 1 word
2) TIMESTAMP TS - 1 word
3) TIMESTAMP FINE - 1 word + 10 words
...
9) ORCOUNTS - 1 word + 10 words
...
14) TRG # ADC - 1 word + 5 words
...
19) TIMESTAMP ADC - 1 word + 5 words
...
24) ADCsamples - 2 words + 320 words

TOTAL= 359 words = 1436 bytes

Figure 3.3: Description of the binary file contents.

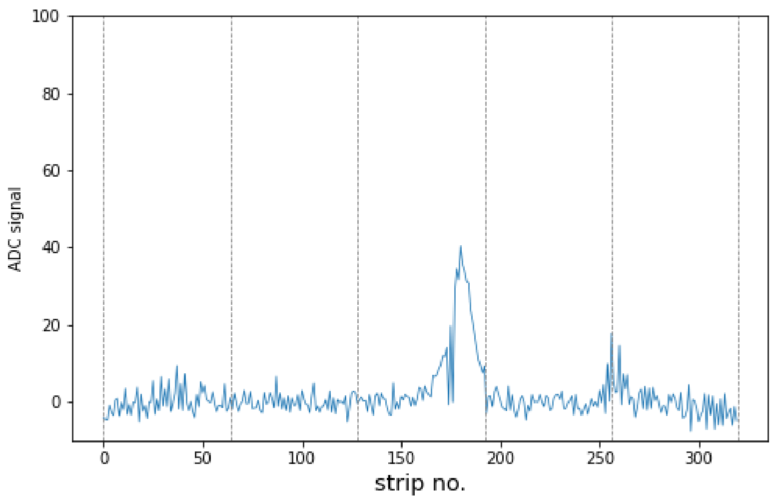

Figure 3.4: ADC signal for one RPC panel. The grey dotted lines show the delimitation of each MAROC.

3.3 RPC Data processing pipeline

Events are selected based on timestamps: all timestamps occurring in a data file are scanned and corrected, see section 3.3.2. The occurrences of each timestamp are counted, and only events with a minimum of 3 hits detected by different boards are processed.

The process is composed of different steps, including consecutive and more accurate estimation for the average signal (pedestal) and the background noise:

- Average signal and standard deviation, representing a first estimation of pedestal and noise, are calculated using all the events recorded by each board.
- Using the first estimation of noise and pedestal, hits are found as signal exceeding $pedestal + 4 * noise$
- Since the presence of a hit causes pedestal over estimation and poor noise calculation, hits found in the previous step are excluded, and a second estimation for noise and pedestal is evaluated.
- Hit finder is run again using the second estimation, and hits are excluded. Pedestal is subtracted from the signal, and “common mode” is calculated as the average signal in each MAROC, and corrected in the pedestal-subtracted signal; the resulting signal baseline should at this point be around 0. The last estimation of the noise is performed
- After pedestal and common mode subtraction, hits are found as signal exceeding $4 * noise$. For each hit, maximum position, start and stop coordinates are stored.

The pipeline can be summarised as follows:

1. first estimation of pedestal and noise item hit exclusion and second pedestal and noise estimation
2. hit detection, pedestal subtraction, common mode correction
3. final noise calculation
4. final hit detection

An example of the hit finding output is shown in figure 3.5.

The pipeline is written in Python; each data file is processed individually and an output text file is produced. The latter contains for each event (timestamp) and readout board (board id), a hit position data structure containing strip number, start and stop. Figure 3.6 shows an example of a detected hit, during three different stages of the pipeline. Corrections are explained in detail in the following section.

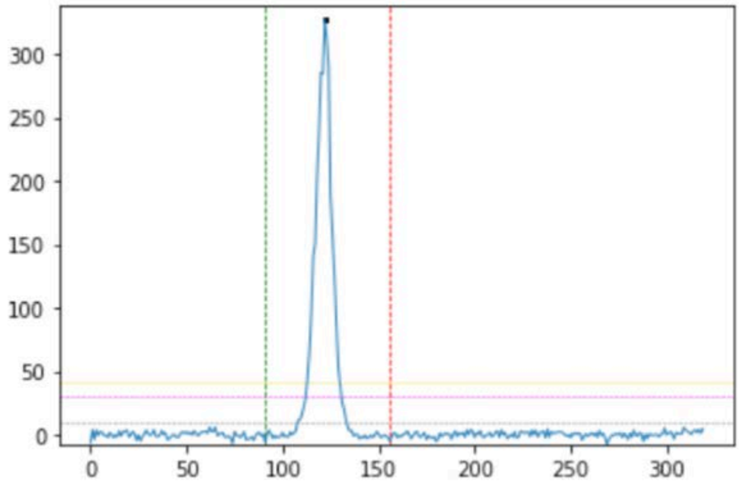

Figure 3.5: Example of hit finder output. The black dot is the detected hit (strip number); the green and red dashed lines are the start and stop strips, respectively; magenta and yellow dotted lines are (3 $*$ $noise$) and (4 $*$ $noise$), used as threshold to detect the hit.

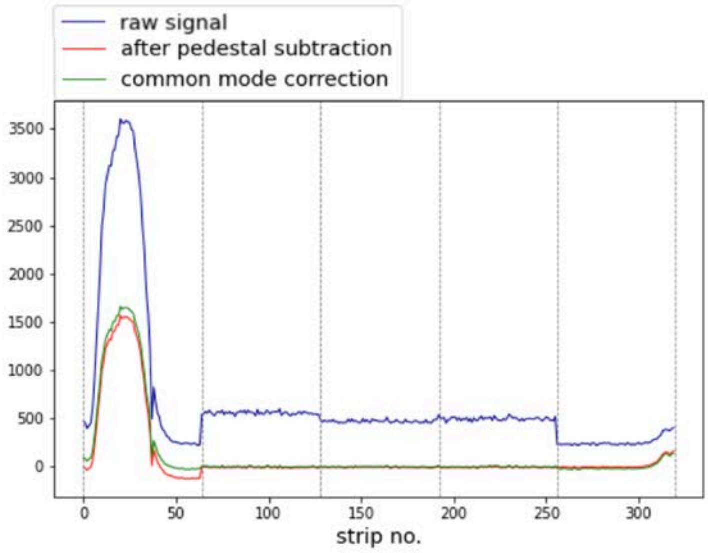

Figure 3.6: An event at different stages in the data processing pipeline.

3.3.1 Data Corrections

Some corrections are needed before applying the hit finding pipeline, and are described in the following sections.

3.3.2 Timestamp corrections

Timestamps are encoded in the int-32 format, starting from a random small non-zero value. A few consecutive corrections are applied to obtain compatible timestamps from all the readout boards.

First event correction

Sometimes, the first event recorded by each readout board is a random value, incompatible with what recorded by the other readout boards. When this happens, the event ID is also different from the expected value (usually 0 or 1). In this case, the first event in the board is skipped, and all event IDs are shifted back to 0. Figure 3.7 shows a zoomed plot of timestamps as a function of the event ID, to draw the attention on the first events, where the issue occurs. While the raw timestamps saved in the files are not exactly the same for all the readout boards, the time difference between each recorded event is the same. To compare timestamps occurring in each readout board, all remaining events, after skipping the first one, are brought to a common start by subtracting the first timestamp. Resulting "corrected timestamps" are now comparable, and differ by ±1 or ±2 at most.

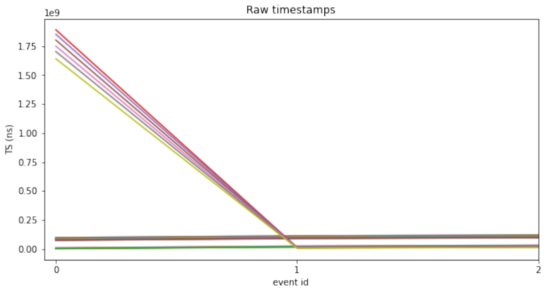

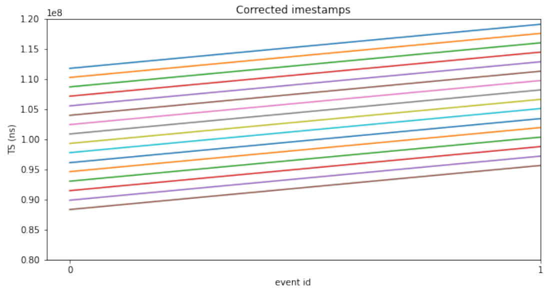

Figure 3.7: Timestamps before first event correction (left) and after skipping the first event (right), showing only the first events, where the issue occurs. Before applying the correction, some boards present a first event with a random high ID, while events from event ID=1 on are correct. After the correction, all events have a common start (event ID=0), and are compatible until the end.

Timestamp overflow correction

It often occurs that during data acquisition the timestamp value reaches 2^{32}, that is the maximum value that can be stored in that numerical representation. When this occurs, the following timestamps in the same data file roll over. After the restart, timestamps are not comparable anymore, as the starting point is different in each board. A second correction is applied, after converting the data to int-64, by adding multiples of the overflow 2^{32}. This is shown in figure 3.8.

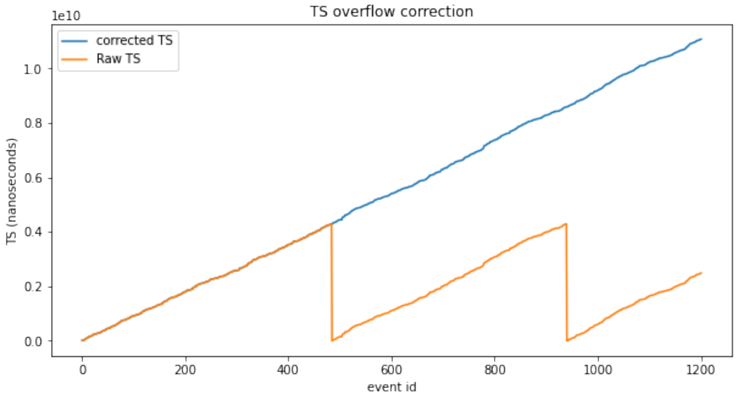

Figure 3.8: Timestamp overflow correction.

3.3.3 Signal overflow correction

The ADC signal is capped at 4096. When in an event the signal in ADC counts exceed that value, the signal for those strips is saved as 0. As this usually happens when a big hit occurs, a correction is needed to recover a hit that would otherwise be missed by the pipeline. A simple workaround is joining the top part of the peak, resulting in a square hit. This can be detected by the hit finder. An example is shown in figure 3.9.

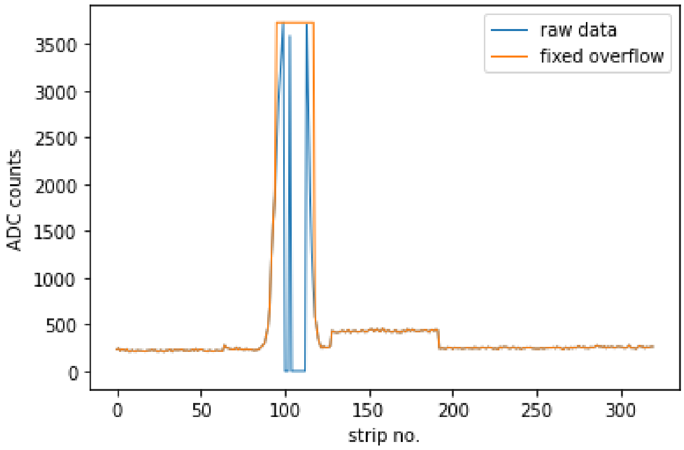

Figure 3.9: Signal overflow correction resulting in a square hit.

3.3.4 MAROC reordering

Some issues in the way MAROC chips are connected to the 64-strip blocks were found, which sometimes resulted in split and misplaced hits between two MAROCs. To solve this, the order in which data is processed from each MAROC is changed in the following way:

$$(0, 1, 2, 3, 4) \longrightarrow (0, 3, 4, 2, 1)$$

Resulting shift of signal hits can be seen in figure 3.10. This improves the hits alignment in consecutive boards, as well as recovering split hits occurring at the edge of consecutive MAROCs.

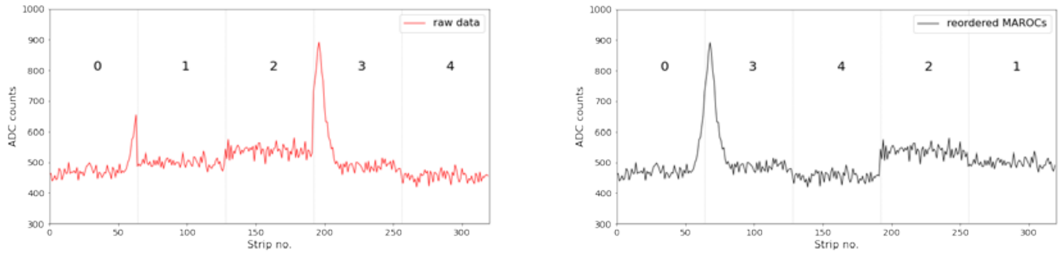

Figure 3.10: An event before and after the MAROC reordering. The reordering recovers a split hit.

3.4 Event Display

Hits on consecutive layers are found by the hit finding pipeline. If more than a chosen number of hits occurs on different panels (usually 3), an event is stored, and can be displayed. An event display is defined, by considering X and Y layers separately. The signal collected by each board is plotted by taking into account the RPC layout in the detector. Since timestamps are used to select the events, if a timestamp is missed by a readout board, that board will not be shown in the display. This representation makes it possible to manually check events with the same timestamps, and see multiple hits by eye. An example of event display is shown in figure 3.11.

3.5 Muon track reconstruction

Muon tracks are found by combining hits on consecutive layers. Hits that are found by the hit finding pipeline are then processed to search for muon tracks. Strip positions are converted to global coordinates (X, Z) and (Y, Z), using the size of each RPC, and their position in the detector. The tracking pipeline is:

- hits are collected in each event;
- global coordinates and layer id are calculated for every hit;
- if more than a given number of layers contain hits (usually 3), a global fit is calculated using all hits;
- if more hits occur on the same layers, all possible combinations of 1 hit in each layer are calculated; of all the global fits, the best, defined as the fit with the minimum chi-square is chosen as the final fit. The slope of the best fit is saved;
- if more than 4 layers contain hits, two local fits, namely top and bottom are
- calculated.

An example of a reconstructed track is shown in figure 3.12.

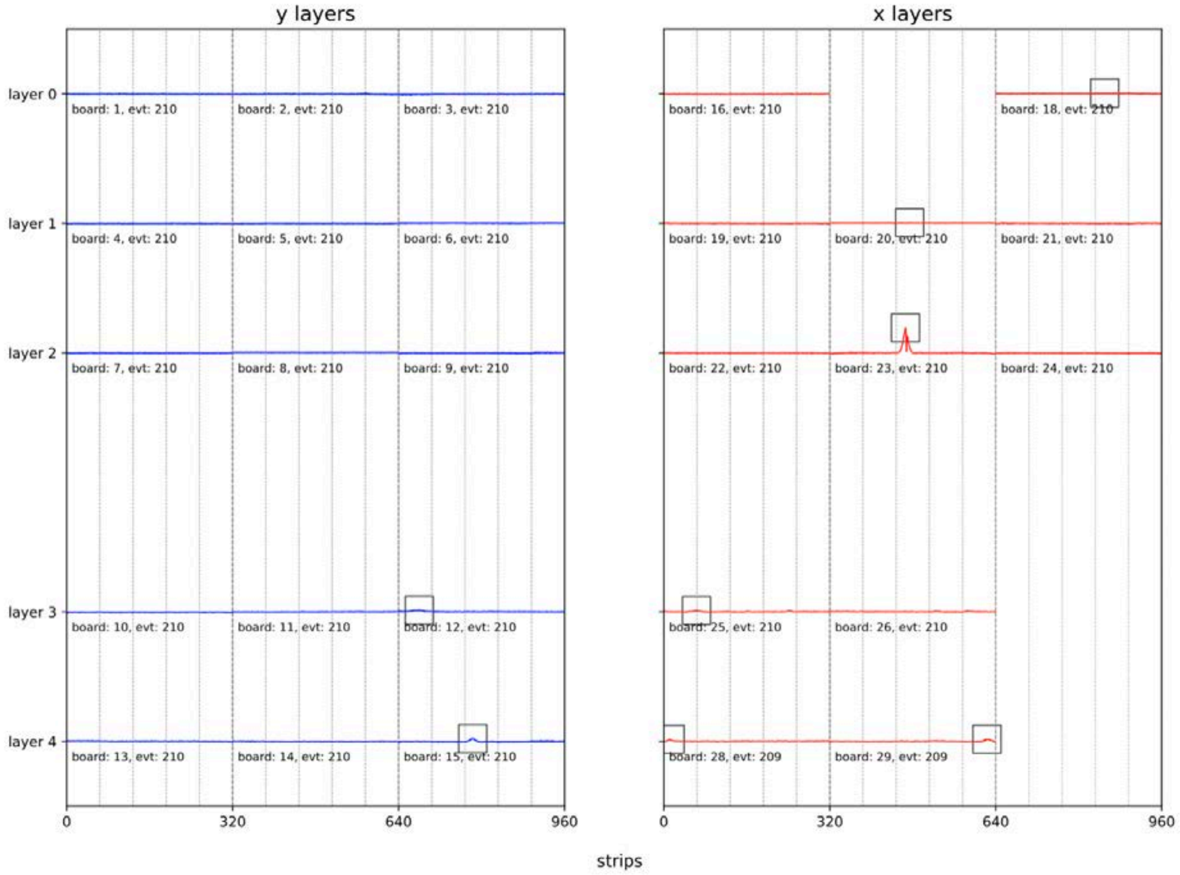

Figure 3.11: Event display. Hits are shown in the two orientations, separately. Detected hits surrounded by a black square. If a Timestamp is missed by a readout board, the latter is not shown in the display.

3.6 RPC performance

Tracks obtained by the analysis pipeline are used to evaluate the detector tracking performance, and the efficiency of each panel by itself. For the results presented here, data collected in 8 months between June 2021 and February 2022 are used. Performance variables like the number of hits per track, the residual distribution and the slope of the reconstructed tracks are shown in the next sections, as well as distribution of hit positions, cluster size, and signal-to-noise plots.

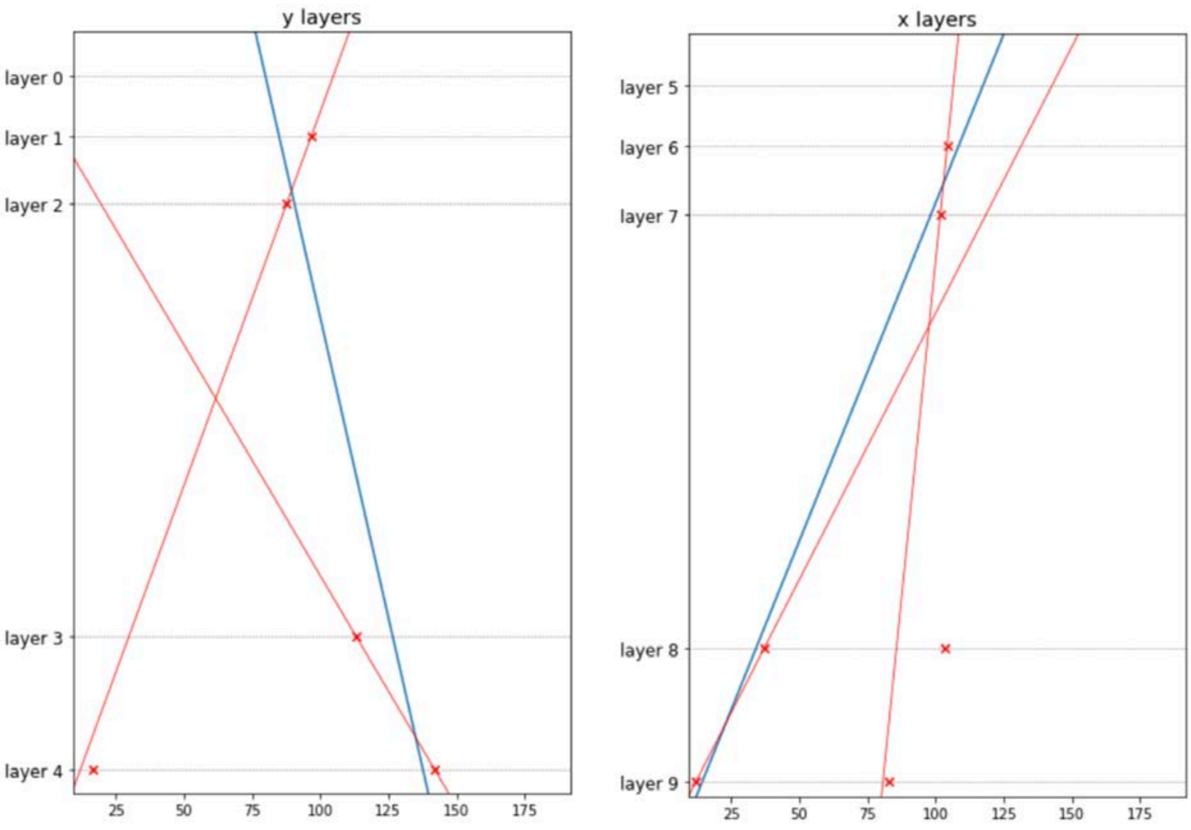

Figure 3.12: Example of a reconstructed track, for y layers (left) and x (layer), respectively. The blue lines are the global fits, calculated using all hits belonging to the "best track"(least $\chi2$), and the top and bottom tracks are shown in red.

3.6.1 Number of hit layers per track

The muon track search starts if at least three different layers have hits. Ideally, good track contains a minimum of five hits, i.e. one per available layer. Around 10 thousand tracks were obtained in the analysed sample. Figure 3.13 shows the distribution of the number of hits per track. The graph shows that the system works well for the detectors in the y-direction, but there is an inefficient layer amongst the detectors in the x-direction. To perform tomography with RPCs only requires at least 4 hits in the xz and in the yz plane.

3.6.2 Residuals distribution

Residuals distributions are calculated to evaluate the how good the hit position reconstruction is. In the case of multiple hits occurring in the same layers, only the hits of the best fit are selected (i.e. the fit yielding the least $\chi2$). The results are shown in figure 3.14, confirming the better performance of the y-layers. However, the distribution is quite wide.

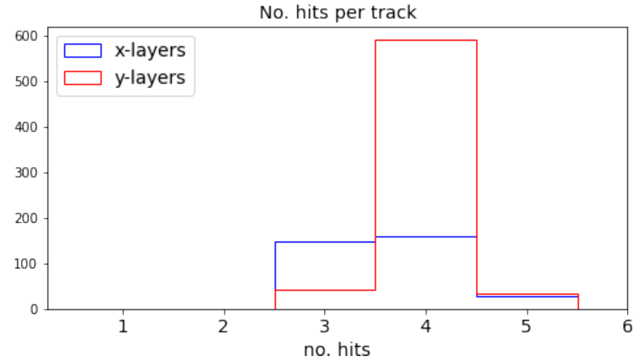

Figure 3.13: Distribution of the number of hits per reconstructed track. There are a few tracks with 5 hits, but most tracks have 4. Y-layers have the highest number of tracks.

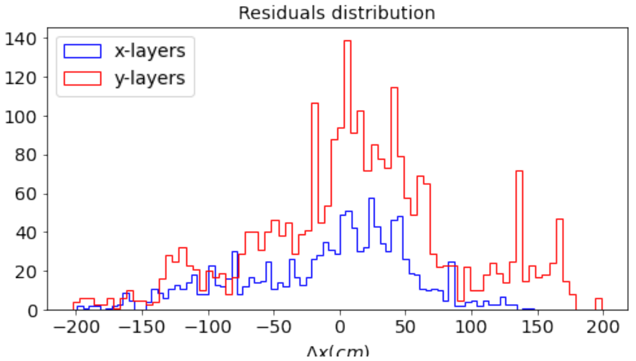

Figure 3.14: Distribution of the global fit residuals.

3.6.3 Slope distribution

For each track, the slope of the global fit is calculated, see figure 3.15, with respect to the horizontal plane. The results show that most tracks are near vertical as to be expected from the muon angular spectrum.

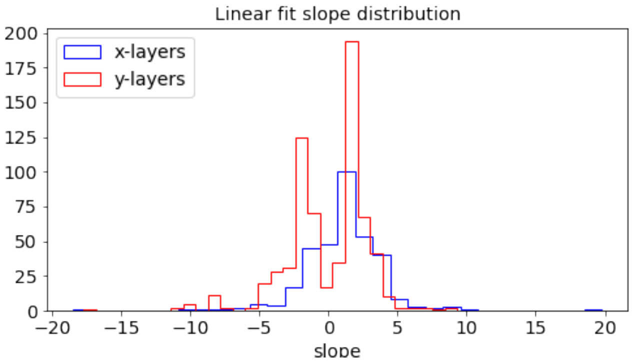

Figure 3.15: Distribution of the slopes of the global fit.

3.6.4 Hit positions

A well-functioning RPC will show a uniform hit distribution throughout the panel, meaning that hits can be detected using every strip. In figure 3.16 the distribution is shown for several RPCs, overlaid with the number of hits belonging to events with at least 3 hits, and to the distributions of hits that belong to reconstructed tracks. Although the latter is expected to be much smaller than the first two, it shows a very low detection efficiency. This analysis also shows that some panels are faulty, or have only one or two functioning MAROCs. Of the 30 initial RPC panels, one was lost due to hardware issues causing the panel to arch when a tension higher than ±2V was applied, and was not included in the analysis as it did not collect any data. 16 of the remaining 29 panels show a reasonable hit distribution but very low efficiency. Four panels appear to have faulty MAROC chips, resulting in missing signal in one or more sections of the panel; and six panels present either a few constantly firing strips, or very few collected hits. An example of each of these behaviours is shown in figure 3.16 (a-f).

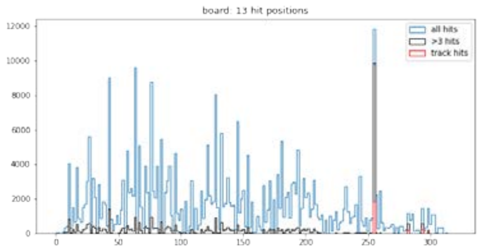

(a)

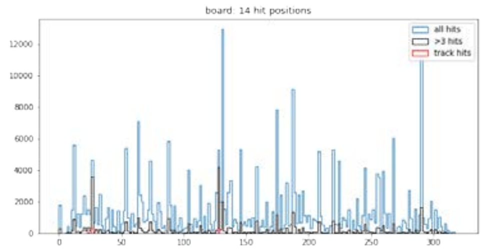

(b)

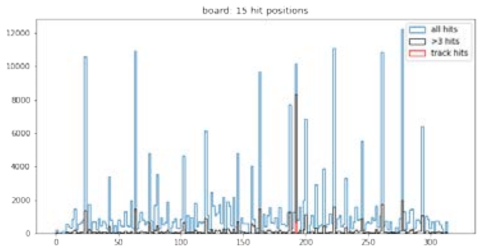

(c)

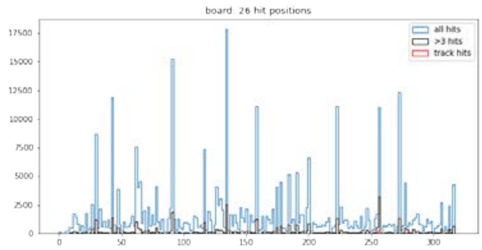

(d)

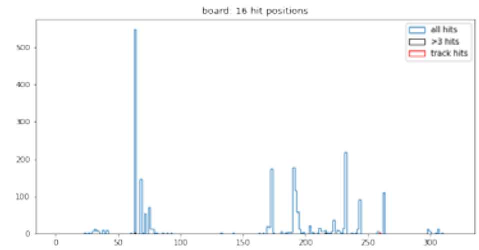

(e)

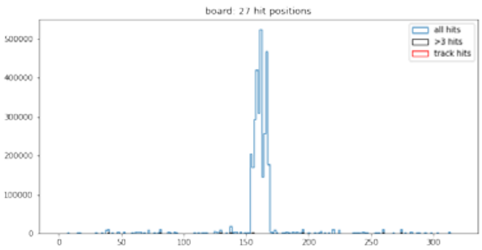

(f)

Figure 3.16: Hit positions distribution for six boards. Some boards behave normally (a-d); others have missing MAROCs (e) or only one functioning MAROC (f).

3.6.5 Cluster size distribution

For each collected hit, the cluster size is calculated as the difference in strip number between the first and the final hit strip, and it represents the width of the hit in number of strips. In normal conditions, each RPC panel shows a wide cluster size distribution, up to the size of an entire MAROC (64 strips wide). Cluster size distributions for a few RPCs are shown in figure 3.17. Most panels collect hits with a cluster size between 20 and 60 strips, except the ones that are not working properly. As will be shown in section 5.3, most RPCs behave well, albeit with the lower efficiency as expected due to the use of CO_2 instead of the R-134a mixture.

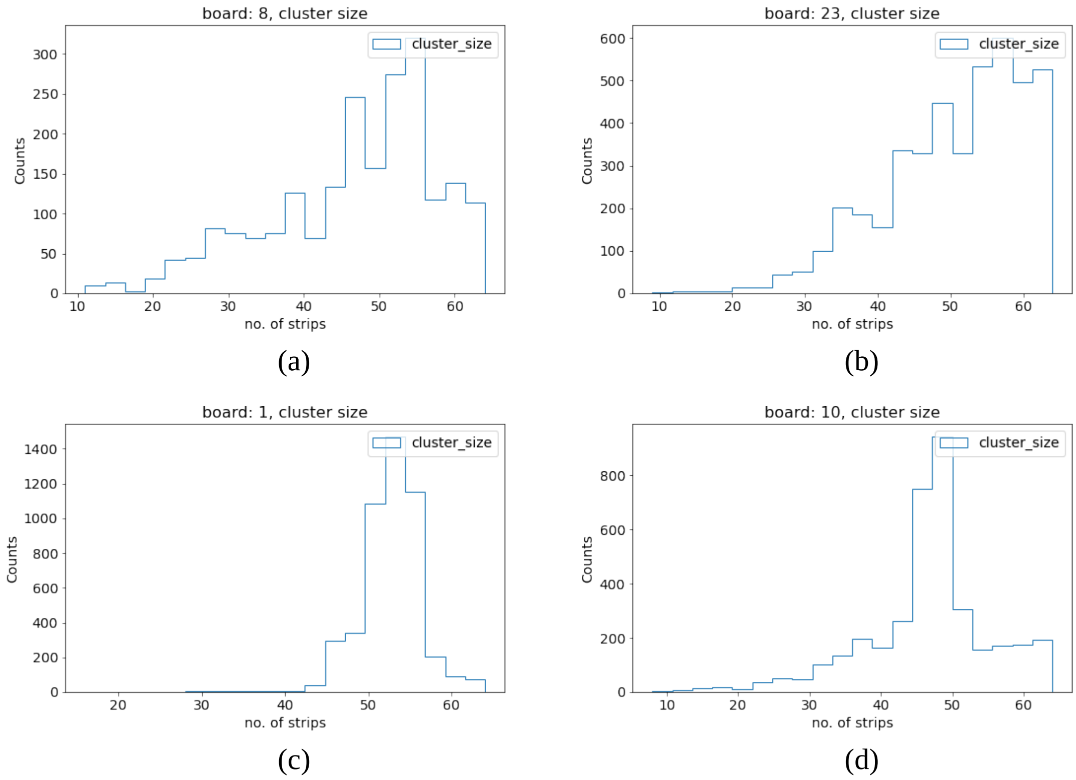

Figure 3.17: Cluster size for four boards. (a-b) are well-behaving RPCs, whereas (c-d) are two cases in which the panel wasn't able to collect many hits, or had malfunctioning MAROC chips.

3.6.6 Signal-to-noise plots

In the absence of an external signal source, like cosmic muons, every strip yields an output that varies according to a Gaussian distribution around the pedestal of a strip. The standard deviation of the distribution is the noise of the strip. Hence, a distribution of A for all events where

$$A = \frac{output_{i,k} - ped_i}{noise_i} \tag{3.1}$$

where the $output_{i,k}$ is the raw output of the strip i in event k and their respective pedestal and noise, a Gaussian with a mean of 0 and a standard deviation of 1 is obtained. The cosmic muons will add positive signals to several strips in each event. Plotting A for each MAROC shows whether the pedestal and noise are calculated correctly and show an excess on the positive side due to signals. Figure 3.18 shows examples of these plots for several RPCs. The graphs for e.g. board 8 show that for all 5 MAROCs the pedestal and noise have been calculated correctly. In addition, the large number of excess hits for MAROC 2 show that a large number of hits will be detected with a > 5σ signal cut. On the other hand, board-1 and board-2 are examples of boards that did not collect many hits due to inefficiencies.

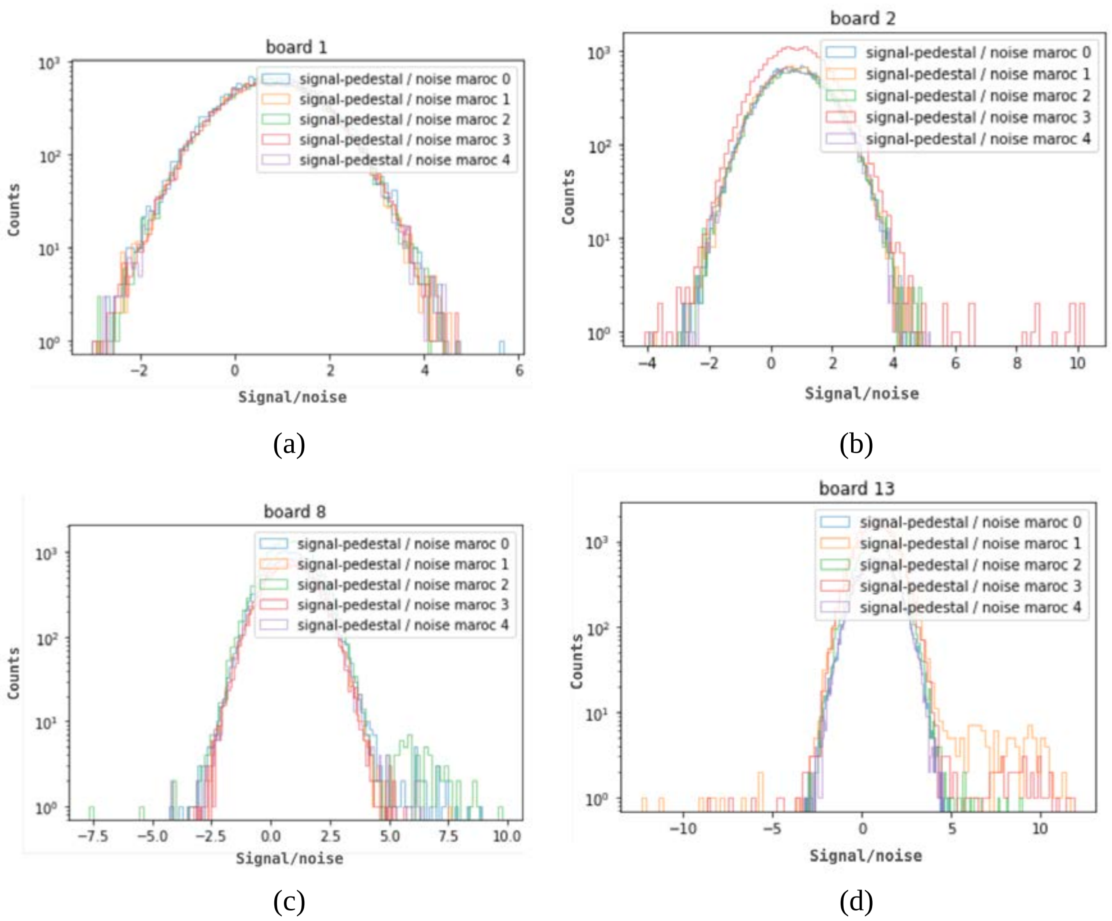

Figure 3.18: Signal-to-noise plots for four boards. (a-b) show cases with none or very few hits collected; (c-d) show well-behaving panels, where collected hits are the tail to the right of the distribution.

3.7 RPC performance summary

As shown here and will be shown in section 5.3, most of the RPCs are working well after solving some minor issues and implementing appropriate corrections. Unfortunately, the hit efficiency is low due to the use of CO_2 as the drift gas. CO_2 provides a signal 5–10 times lower than R-134a. This could only be recovered to a small extent by an increase in high voltage. We used the highest voltages possible below break down.

4. Drift Chambers

The CHANCE Drift Chamber tracking system provides a measurement of the muon trajectory below the region of interest by reconstructing the muon crossing position across 6 layers of drift planes. Each of these drift planes consists of three individual 60 cm × 180 cm drift chambers placed next to one another to form a 180 cm × 180cm detection plane.

4.1 Operating Principle

The 60 cm × 180cm enclosed drift chambers used in the CHANCE detector allow the detection of a muon crossing position with approximately 2-3 mm resolution by measuring the time taken for ionisation electrons produced inside the chamber to drift to a centrally located anode wire. As shown in in figure 4.1, a cathode plane shapes the electric field in each chamber to produce a stable electric field up to 30cm away from the anode wire. The gas volume inside each chamber is flushed with a mixture of 5% CO_2, 2.5% Methane, and 92.5% argon, which provides a stable drift velocity over a wide range of electric field strengths. Typically, operating voltages of 5575 V on the anodes and 3800 V on the cathode are used, resulting in a stable electric field strength of 126 V/cm in the drift region. Knowledge of the electric field strength can be used to infer the drift velocity of electrons in a gas, however typically the maximum time taken for drift electrons to arrive at the anode wire is used to extract this velocity empirically during data taking.

If the original time the muon crossed the chambers is known, for example from an external trigger, then the time difference between the crossing time and the time of arrival for the electron drift cloud, provides a process measurement of the crossing position. Each chamber has a built in preamplifier circuit next to its high voltage feed throughs that converts the drift electron signal on the anode wire to a voltage output pulse for recording by a digitiser or oscilloscope.

Because of the long drift distances only a single readout channel, is needed for a 60 cm wide chamber. This makes single wire drift chambers an economical way to instrument large area muon tracking systems. The two drawbacks in this long drift distance design is that a oxygen ingress in each chamber needs to be kept to a minimum, and no information is available on whether the drift electrons came from the left or right side of the wire. This creates what is referred to as “ghost” hits in the chamber. This is corrected for by introducing a 3 cm offset between drift chamber layers on consecutive layers. This offset can be used to distinguish individual tracks as typically for muon candidate events only a single combination produces a valid straight line fit result. The track residual, the average distance between each hit identified hit and a straight line fit, is used to identify the combination of drift chamber hits most likely to be due to a crossing muon. As shown in figure 4.2, due to the relative chamber offsets in the middle layer, only a single combination of hits produces a straight track pointing to the right with a low track residual. Without this offset, two tracks one pointing left and the other pointing right, would both be equally valid straight tracks with no possible way to discriminate which was the true muon trajectory.

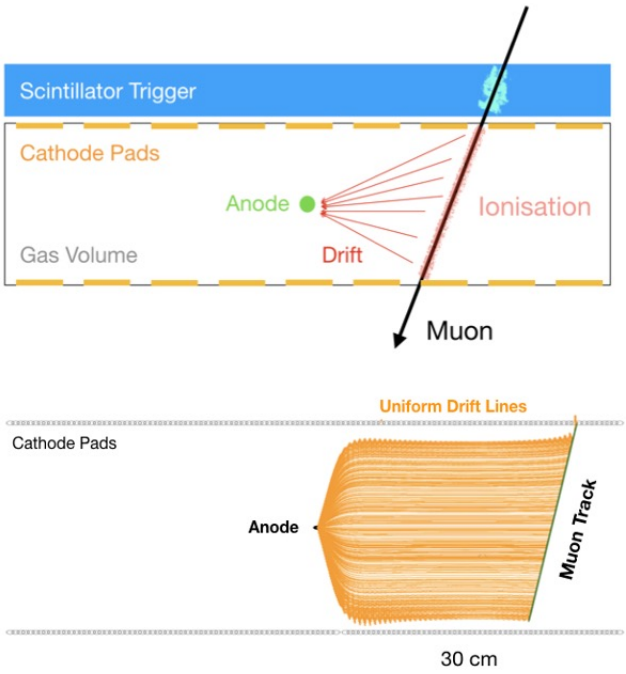

Figure 4.1: (Top) Drift chamber operating principle. Muons produce ionisation electrons inside the drift gas volume, which drift in a constant electric field to centrally located anode wire. The time taken to reach the anode wire, relative to an external scintillator trigger time, is used to infer the muons crossing position. (Bottom) Equally spaced cathode pads at voltages starting at 3800 V that drop with distance from the central anode, results in a uniform drift field with smooth drift lines leading toward the centre of the chamber.

4.2 Drift chamber data acquisition

The signal outputs from each of the 18 drift chambers are readout passed to two separate 9 channel preamplifier units which amplifies the signal by a factor of 20, before being readout by a 32 channel 62.5 MSps DT5740 CAEN digitiser. The DT5740 is configured to record 4096 ADC samples for each channel following an external trigger, corresponding to a maximum drift time of approximately 65us.

Example data readout from the DT5740 digitiser is shown in figure 4.3, showing the incoming pulses appearing at later times from separate drift chambers following an external trigger.

Due to the large file sizes created by reading out such a large data window for each event, the data is compressed to the bare minimum amount of data needed to reliably re-construct muon tracks. Assuming that only one muon crosses a drift chamber within the time window following an external trigger, the maximum ADC sample measured, and when it occurs within the timing window, are the only pieces of information saved for each channel per event. This is sufficient to convert the digitiser into a simple time-to-digital convertor, with the triggering thresholds for each channel being allowed to be set after data collection has taken place.

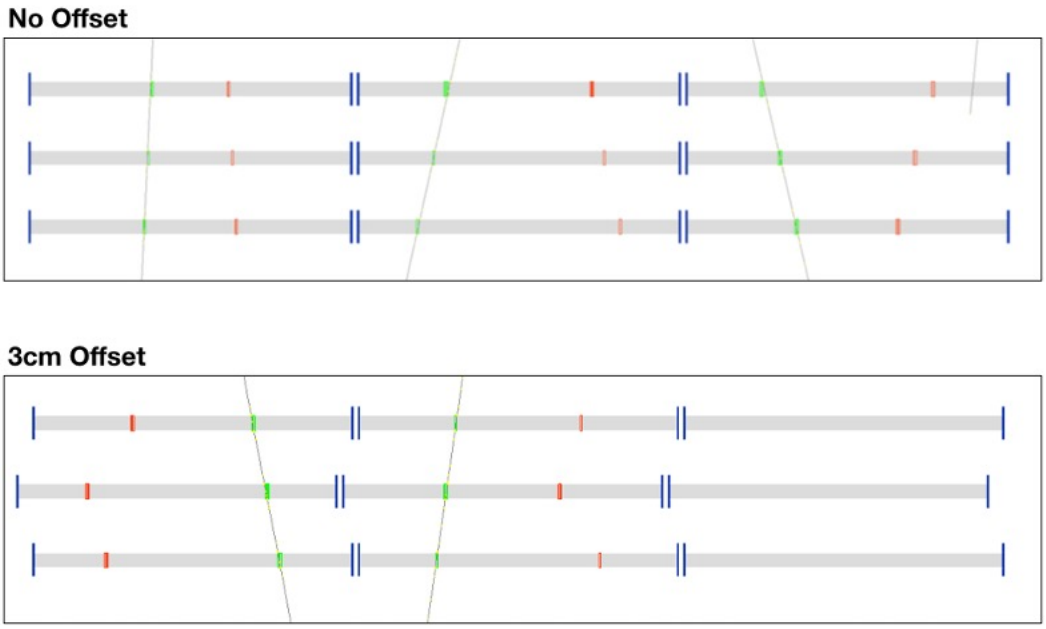

Figure 4.2: Track reconstruction example for a drift chamber subsystem. The true (green) and ghost (red) hit positions are shown for example MC simulation events. As shown in the top figure, without any chamber offset, based on the hit positions alone there is no way to distinguish which is the true muon trajectory. As shown in the bottom figure the introduction of a 3 cm middle layer offset allows the tracking residual to be used to distinguish the true muon trajectory by looking for a straight line fit.

The DT5740 and associated software toolchain is setup to automatically segment files into smaller chunks to make them easier to process, before automated scripts are used to convert the output data files into ROOT TTree files, that are 2% lower smaller the starting files. The final data output from the system that could be used to produce tracks after this compression stage is approximately 5KB/s (450MB/day), small enough that a wireless hotspot would be sufficient to monitor the data output coming from the system from a remote location. Since August 2019, all data-taking and processing from the drift system has been remotely controlled from Sheffield through a 3G-enabled hot spots with fixed IP.

4.3 Hit Position Finding

Event samples containing the maximum ADC value on each channel within the timing window need to be further processed to produce valid hit positions. Because the digitiser software saves the first time the maximum 12-bit ADC value occurs, there is a natural bias for noise hits due to baseline tipple to occur at the start of the timing window as shown in the trigger time distribution in figure 4.4. The region of interest for the drift chamber readout shown in figure 4.4 is between samples 400 and 2000. Additional data is taken outside of this region of interest during normal operation so that a baseline fit can be performed to determine the natural slope in the trigger time distribution and remove it.

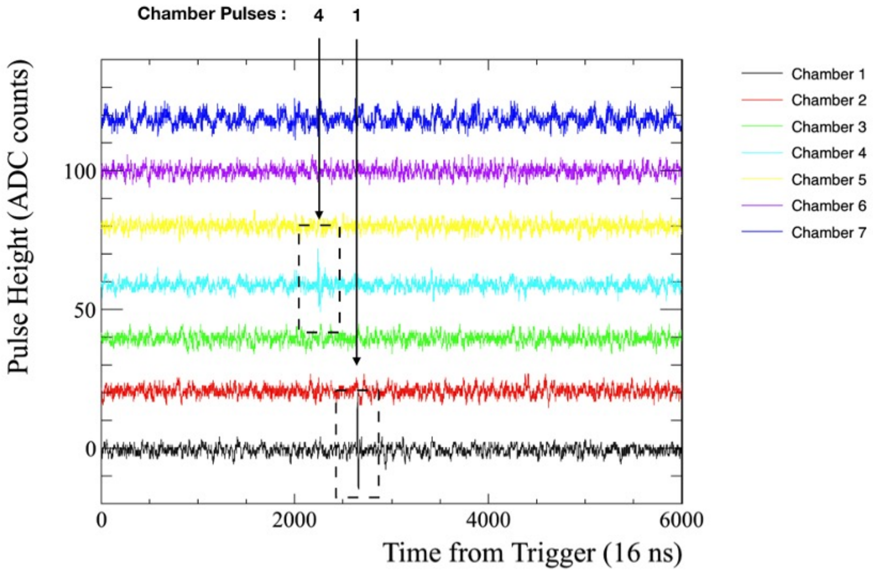

Figure 4.3: Example pulses from seven of the individual drift chambers. Chambers 1 and 4 (directly above one another), have both triggered at slightly different times, likely due to a high angle track. Given the large timing window necessary to readout each chamber, it is not feasible to save the entire 6000 sample long pulse for each event.

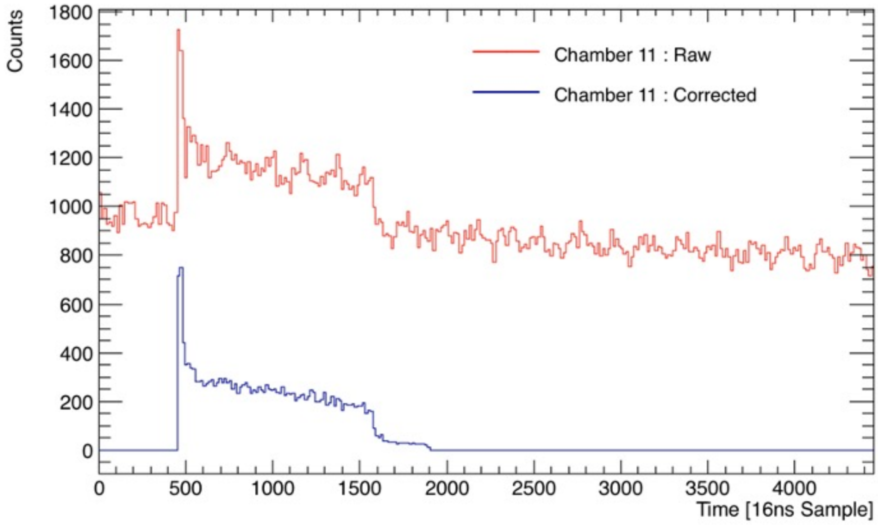

Figure 4.4: Drift chamber timing distributions before and after baseline and maximum ADC value corrections.

The natural baseline ripple is also clear in the raw data in figure 4.4. This is corrected for by placing a cut on the minimum ADC value that constitutes a hit. This cut value is automatically placed 30 mV above the average baseline ADC value for each channel. Finally, cuts are placed on the minimum and maximum time relative to the external trigger, to rejects drift evens that should not be associated with the given trigger due to noise or back-ground pileup. As shown in figure 4.4, the addition of these cuts produces a corrected timing distribution with a flat timing distribution corresponding to a uniform drift velocity when moving away from the anode wire.

After these corrections, hit positions are obtained by simply multiplying the drift time (the time of each triggered channel relative to the external trigger time), by the chamber drift velocity, 0.0126 cm/ns. This velocity is obtained empirically from the data for each chamber, by looking at the maximum drift time obtained during normal operation and averaging across all chambers. Example converted drift positions obtained for one chamber are shown in figure 4.5. The final distribution is a flat distribution extending out to ±33cm away from the anode wire. It is exactly symmetric due to the lack of knowledge of whether any hit occurred on the left or right side.

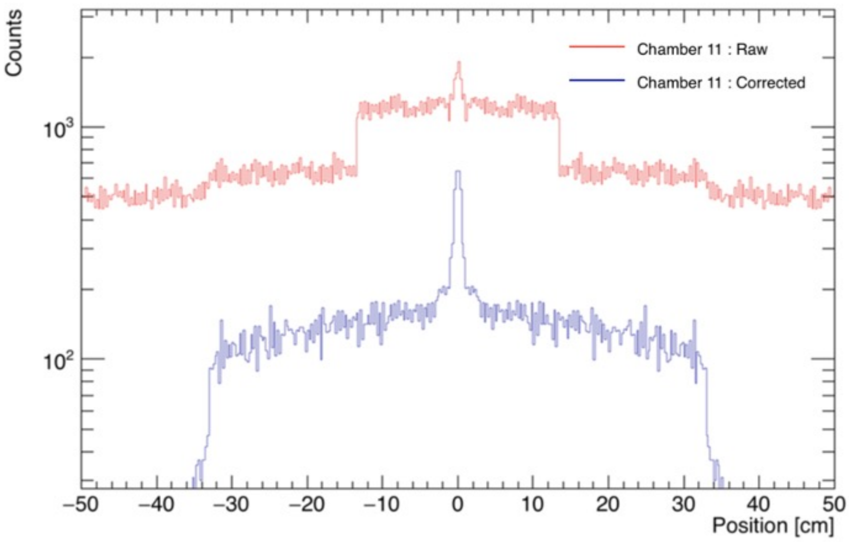

Figure 4.5: Drift chamber timing distributions before and after baseline and maximum ADC value corrections.

As discussed earlier, following the conversion of drift times into possible hit positions, an additional tracking residual cut is then needed to determine the true muon trajectory. Figure 4.6 shows an example of one of these track fits for real data, with chamber positions overlaid on top.

4.4 Deployment issues

After our initial commissioning phase, a drift chamber plane developed a problem. It was decided to replace this layer by a new drift chamber. This new layer first needed to be produced and then installed.

Later on a drift chamber layer developed problems. It was decided not to replace it by another drift chamber but by another layer of RPCs. This caused delay as the RPCs needed to be produced from the bare glass RPCs. The installation of the layer was delayed as the connectors were not available due to Brexit. When they became available, installation was not allowed as the country was in lock down and covid access restrictions applied. In the final operational phase of the system, data was taking with 5 layers of RPCs and one drift chamber. The choice was mainly motivated by the need to get the system up and running again as soon as possible. At the time, the drift chamber experts from the University of Sheffield were not allowed to travel to Bristol due to UK government covid-19 policy. As such, we had no alternative. It would have been more beneficial to replace the drift chamber by another drift chamber if we could have been sure that the experts could visit the system to install the new drift chamber.

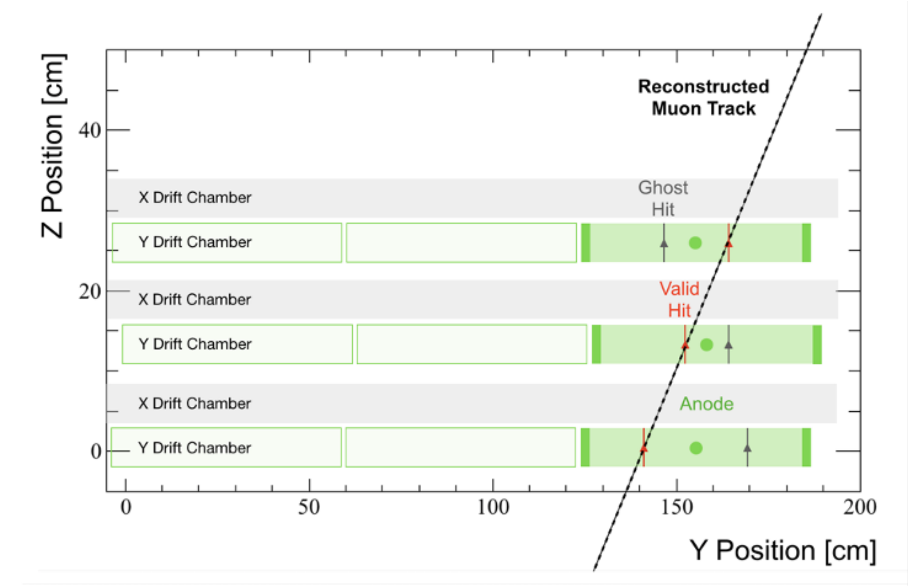

Figure 4.6: Track reconstruction example for the drift chamber subsystem. The valid and ghost hit positions are taken from an example event in the real system data. The extent of each chamber and approximate location of its anode wire has been overlaid on top. The combination of hits highlighted in red are the only ones that have an average track residual less than 3 mm.

5. Global Tracking

Due to differences in the control software between the RPC and Drift Chamber subsystems data acquisition is kept separate up until the global matching and track fit stage. Data is obtained independently from both systems, with their trigger indices are kept approximately synchronised by sharing a common global trigger from the discriminator unit. This allows an additional data processing stage to be run offline to match up the data from both subsystems before reconstructing global tracks of the muons trajectory above and below the imaging volume. The offline process is split into 3 stages; trigger matching, locale track fitting, final global point-of-closest approach calculation.

5.1 Event Trigger Matching

The global trigger system keeps the total event count between the RPC and Drift System approximately synchronised, however due to unexpected delays in data acquisition occasionally either system can miss a global trigger input. Most commonly this occurs due to a reconfiguring of the RPC front end boards after each new data file. Since the front ends of the drift chambers are analogue only, and the data acquisition of the drift chamber system is performed on a single 32 channel event buffering digitiser. This problem is less common for the drift subsystem. The trade-off between the two is that the drift chamber system is far less portable and reconfigurable than the RPC system due to lack of integrated front end boards.

Build up of trigger “misses” on either system due to unsynchronised dead time result in a gradual drift in the trigger count on the drift chamber system relative to the RPC system that must be corrected for. This is possible by recognising that aside from regions where the system is in a unsynchronised dead time state, the time difference between two consecutive triggers inputs should be the same on both subsystems. Therefore, if graphs of the time differences between triggers are created for small subsets of the RPC event sample (typically 100 events), it is possible to find a matching timing graph within the Drift Chamber event sample. These timing graphs are referred to as “timestep signatures”, and are shown in figure 5.1.

An automated timestamp signature matching procedure has been developed that can reliably match the trigger indices between the RPC and Drift Chamber Systems and output combined hit position data for further processing. The trigger matching efficiency is found to be 96.4%, where the 4% drop in efficiency comes from missed events at the start or end of the RPC data stream due to unsynchronised system dead time.

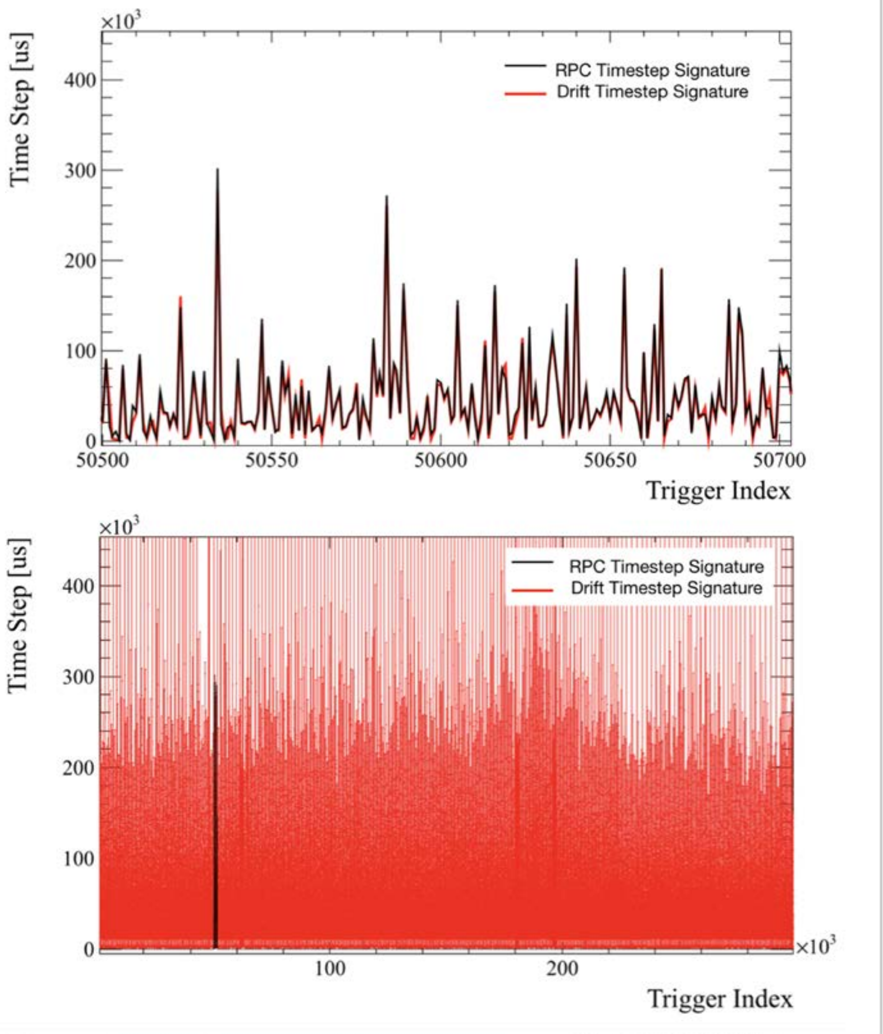

Figure 5.1: (Top) Example time step signature for a small sample of RPC events showing the correspondence obtained when the trigger indices are in sync. (Bottom) Trigger synchronisation is achieved by scanning all possible trigger indices within a drift chamber output file and finding where the RPC time step signature closely matches.

5.2 Global Track Fitting

Global Track fitting is performed in a similar fashion to each subsystems individual track fitting. First hits are divided into corresponding “locales”. These are top-X, top-Y, bottom-X, and bottom-Y respectively. An individual track fit is then performed in each of these locales to obtain the 1D track gradient and vertical offset, before these are merged to form a 3D muon trajectory above and below the imaging volume. Whilst a global track fit could be performed in 3D space to try to obtain a scattering point within the imaging volume, this split-locale approach allows us to also consider events that may

have formed a valid track in 2 of the 4 locales and attempt to use this information to improve the speed at which a useful imaging data set could be obtained.
For the top-X, top-Y, locales, only a two RPC layers are present, therefore the track fit is a simple straight line approximation between the obtained hit positions within each log-scale. The bottom-X and Y locale track fit is slightly more complicated due to the inclusion of three additional drift chamber layers. Inclusion of these layers is important as the drift chambers in the bottom-Y locale provide additional 3-point tracking information, allowing a confirmation that the detected tracks are indeed due to a crossing muon. Since the drift chambers provide two possible hit positions (a normal and a "ghost" hit), the trackfit must consider all possible hit combinations for the bottom-X locale before choosing a track with a tracking residual less than a chosen threshold.

5.3 Implementation

We developed the global track fit at the beginning of the project, when we were expecting to run with R-134a for the RPCs and thus a large amount of good tracks. After installation of the system and suffering from the R-134a ban, see section 3.1, our efficiency was lower than expected. In addition, the drift chambers developed issues and in the end one was replaced by an additional RPC layer, see section 4.4.

Around that time, we identified the RPC timing issue, see section 3.3.2. After solving that and the fifth RPC layer was installed, it was more practical to perform tracking with initially the RPC system only and later on combine the drift chamber information. Figure 5.2 shows an overview of the tracking performance for each RPC. It shows for each RPC how often it was part of a full 5 hit track, how often it was part of a 4 hit track, how often it was missing on an otherwise good 4 hit track, how often it was part of a 3 hit track, how often it was missing on an otherwise good a 3 hit track. Ideally, all RPCs are only part of good 5 hits tracks, but this is clearly not the case. Some RPCs are not responding well and are not often recording a hit, for example RPC 16 and 17, while RPC 2, 6 & 7 are showing a lot of hits on 4 hit tracks. The results indicate that we have recorded a small but good sample of tracks, but also that there are parts of the detector system that do not provide (many) hits.

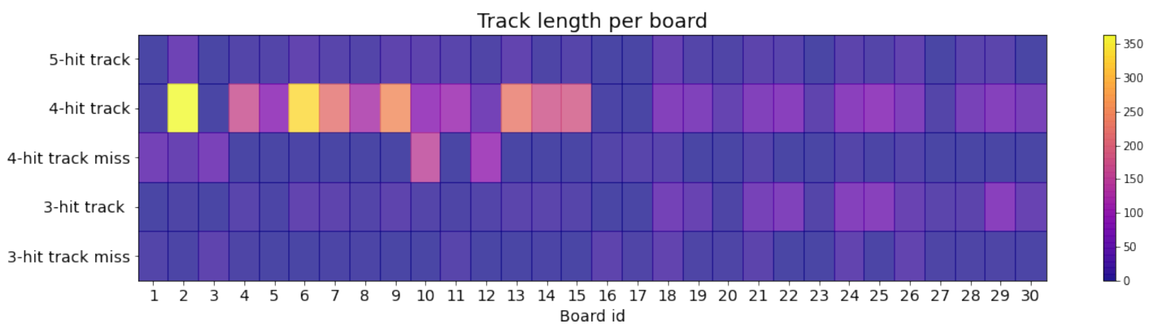

Figure 5.2: Heatmap showing for each board the length of the track it belongs to. Most tracks have 4 hits, and the Y layers have a higher detection efficiency than the X ones. Missing hits are also shown in the 5-hit track and 4-hit tracks case.

6. Challenges

As reported during reporting cycle, we have experienced several major challenges severely affecting our experimental programme. We have tried to mitigate their effects to the best of our abilities and pushed to get the best possible results out of the system before the end of the project. Unfortunately, we were not successful and have only managed to obtain a small sample of muon tracks.

We have reported the causes for our delays and difficulties in the CHANCE progress reports. Here is an overview of the key challenges.

- Our foremost problem with the RPC system was the chance in environmental regulations preventing us from using Freon, see section 3.1. Freon is an excellent gas for RPCs. When running our pre-CHANCE prototype with Freon, chamber efficiencies of well over 95% were obtained, see chapter 3. Freon yields on average 81.6 electron-ion pairs are produced per mm as primary ionisation, which then multiply while travelling through the gas gap. We needed to switch to CO_2 which only has an average of 35.5 electron-ion pairs are produced per mm as primary ionisation and 91 electron-ion pairs are produced per mm in total. This results in most probable signal of a factor 5 – 10 lower than when using Freon and thus a major decrease in efficiency. Other allowed gasses have similar performance to CO_2. To get a permit to run with Freon would have required the purchase of an abatement system. We requested an indicative quote and the price was close to £200,000. We could not afford to buy this system. The lower efficiency is the thing that harmed our experimental programme most. Ideal tracks that have recorded hits in all 12 layers (6 in the xz and 6 in the yz plane) are rare if the efficiency is small. The fraction of tracks that has hits in all 10 RPC layers is given by ε^{10}, where ε is the efficiency. Clearly, unless the efficiency of all planes is very high, very few muon tracks will be recorded, as indicated in the tableau below.

ε (%)	Track fraction (%)
99	90.4
98	81.7
95	59.9
90	34.9
80	10.7
70	2.8
50	0.98

- Initially, we suffered delays to get Health & Safety approval for our system as installed in the barn. There were questions about the strength of the mechanical supports and the safety of the high voltage system. The mechanical structure was deployed for a similar system before but came without the required paperwork. The design for our high voltage system was used before at the University of Bristol for our pre-CHANCE prototype system. Nevertheless, it took weeks before we got approval to turn on the system.

- After our initial commissioning phase, a drift chamber plane developed a problem. It was decided to replace this layer by a new drift chamber. This new layer first needed to be produced and then installed.
- The photomultiplier tubes were found to have a low efficiency and were replaced.
- The system was installed in a grain barn at Fenswood farm. During CHANCE the system needed to be moved from the grain barn to the main barn. This meant disassembling the system and reinstalling and recommissioning it. This took 2–3 months.
- A high voltage power supply module for the RPC system broke. Replacing this took 10 weeks.
- A drift chamber layer developed problems. It was decided not to replace it by another drift chamber but by another layer of RPCs. This caused delay as the RPCs needed to be produced from the bare glass RPCs. The installation of the layer was delayed as the connectors were not available due to Brexit. When they became available, installation was not allowed as the country was in lock down and covid access restrictions applied. The choice was mainly motivated by the need to get the system up and running again as soon as possible. At the time, the drift chamber experts from the University of Sheffield were not allowed to travel to Bristol due to UK government covid-19 policy. As such, we had no alternative. It would have been more beneficial to replace the drift chamber by another drift chamber if we could have been sure that the experts could visit the system to install the new drift chamber.
- We discovered a feature in the time stamping of the RPC data, see section 3.3.2, quite late on in the project. This feature did not affect data taking with our pre-CHANCE RPC system. In that system we relied on the trigger number, which was the same for each RPC. Hence, the RPC events in different RPCs were always combined correctly. To merge the data with the drift chambers required usage of the actual time stamp, which showed the feature.

Besides the challenges associated to technical development, some issues were faced due to the covid crisis even if the project had been extended and the Brexit, namely:

- Key staff left during the project, in particular the PDRAs Dr Kopp, Dr Stowell and Dr Barker. A key responsibility of Dr Kopp's was to keep the system running. Dr Kopp left during the first UK lockdown of the covid crisis. The University of Bristol had a hiring stop. As such it took a few months to replace Dr Kopp. Dr Stowell was the expert for the drift chamber system and analysis. He was replaced by Dr Barker, who left later on in the project.
- During the covid lock downs staff from the University of Bristol had permission to keep the system running, but we were not allowed to do significant amounts of work on the system and were not allowed in the building where the spare parts were located. The University of Sheffield staff was not allowed to attend the system at all. This lead to significant delays as we could not fix and optimise minor issues.

Despite suffering these issues, we did build and successfully operate a muon tomography system consisting of RPCs and drift chambers as planned in the proposal. Our main issues: the R-134a ban, the covid pandemic with all travel and staff operations issues and Brexit related problems, could not have been foreseen at the start of the projects. These have made the practical part of the project extremely challenging but we did manage to deliver a working system.

7. Summary

In the Muon Tomography work package of the CHANCE project, we set out to build and operate a muon tomography system using RPCs and drift chambers. The system was intended to be mobile system to be operated in a non-laboratory environment. We have built and successfully operated this system. It was operated in two different barns at Fenswood farm, a University of Bristol owned farm. The system was moved between the two barns, showing that it is mobile.

The project has not been without challenges. We have extensively reported on them in this report and continuously during the project. Our main issues, the new environmental regulations banning the use of R-134a, Brexit related problems and the covid pandemic with all travel and staff operations issues, could not have been foreseen at the start at the project nor mitigate against. The extension of the project did compensate the latter two issues to some extent.

We were taken by surprise by a ban on the use of R-134a. Our RPCs leak a small amount of this to the atmosphere, but a blanket ban on R-134a came into force in the UK. This made it impossible to purchase R-134a without the appropriate permit, which we could not get. Installing an approved abatement system would have cost ~£200,000 plus installation cost for site engineering. This was not feasible within the restrictions of the CHANCE project.

During the covid pandemic, it was not possible to do work on the system. University of Bristol staff had no permission to enter the building with the spare parts and University of Sheffield staff were not allowed to travel to Bristol to work on the system and thus could not work on the system either. Furthermore, key staff left and we were not allowed to hire replacement staff as the University of Bristol was concerned about its financial health. The hiring ban delayed the replacement of the key personal by a few months. When the covid situation improved, it was still complicated to get spare parts delivered on site. We did manage to keep the system running but it did not perform well at that time.

Brexit also meant that we had limited access to spare parts. For example, a high voltage module broke and needed to be sent for repair. Before Brexit, this would have taken 2 weeks. Now it was 10 weeks. Basic connectors were no longer available and so on.

Despite all these issues that have made the practical part of the project extremely challenging, we did manage to deliver a working system. We pushed the data taking as long as we could to improve our data sample and thus imaging capability.

8. Bibliography

[1] Simon Eidelman et al. “Review of particle physics”. In: Physics Letters B 592.1 (2004).
[2] C.L. Morris et al. “Tomographic Imaging with Cosmic Ray Muons”. In: Science and Global Security 16 (2008), pp. 37–53.
[3] A. Kopp et al. “Non-destructive assay of nuclear waste containers using muon scattering tomography in the Horizon2020 CHANCE project”. In: EPJ Web Conf. ANIMMA 2019 – Advancements in Nuclear Instrumentation Measurement Methods and their Applications 06008 (2020).
[4] A. Simpson et al. “Muon tomography for the analysis of in-container vitrified products”. In: Appl. Rad. Isot. 157, 109033 (2020).
[5] P Baesso et al. “Toward a RPC-based muon tomography system for cargo containers.” In: Journal of Instrumentation 9.10 (2014), p. C10041.
[6] P Baesso et al. “A high resolution resistive plate chamber tracking system developed for cosmic ray muon tomography”. In: Journal of Instrumentation 8.08 (2013), P08006.
[7] P. Baesso et al. “Degradation in the efficiency of glass Resistive Plate Chambers operated without external gas supply”. In: Journal of Instrumentation 10 (June 2015), P06001–P06001. doi: 10.1088/1748-0221/10/06/P06001.
[8] D. Cussans et al. “A readout system for a cosmic ray telescope using Resistive Plate Chambers”. In: JINST 8 C03003 (2013).
[9] S. Blin et al. “MAROC, a generic photomultiplier readout chip”. In: IEEE Nucl. Sci. Symp. Conf. Rec. 1690 (2010).
[10] R. Frazier et al. “Software and firmware for controlling CMS trigger and readout hardware via gigabit ethernet”. In: proceedings of the 2nd International Conference on Technology and Instrumentation in Particle Physics (TIPP 2011), Phys. Proc. 37 1892 (2012).
[11] Rick Bitter, Taqi Mohiuddin, and MattNawrocki. LabVIEW: Advanced programming techniques. Crc Press, 2006.
[12] G. Saviano et al. “Properties of potential eco-friendly gas replacements for particle detectors in high-energy physics”. In: Journal of Instrumentation 13 (2018), P03012.
[13] Archana Sharma. “Properties of some gas mixtures used in tracking detectors”. In: SLAC-J-ICFA-16-3, SLAC-JOURNAL-ICFA-16-3 (July 1998).
[14] X. Fan et al. “Precise measurement of gas parameters in a realistic RPC configuration: The currently used R134a gas and a potential alternative eco-gas”. In: Nuclear Instruments and Methods in Physics Research Section A: Accelerators, Spectrometers, Detectors and Associated Equipment 1024 (2022), p. 166124. issn: 0168-9002. doi: https://doi.org/10.1016/j.nima.2021.166124. url: https : / / www . sciencedirect . com / science / article / pii / S0168900221010202.
[15] G. Rigoletti et al. “Studies of RPC detector operation with eco-friendly gas mixtures under irradiation at the CERN Gamma Irradiation Facility”. In: Proceedings of Science 364 (2020).
[16] M. Kang et al. “Study of eco-friendly gas mixtures for SHiP RPCs”. In: J. Korean Phys. Soc. 80 (2022), pp. 1–12.

EPJ Web of Conferences **225**, 06008 (2020) https://doi.org/10.1051/epjconf/202022506008
ANIMMA 2019

Non-destructive assay of nuclear waste containers using muon scattering tomography in the Horizon2020 CHANCE project

Anna Kopp[1*], Ahmad Alrheli[2], Daniel Kikoła[3], Mohammed Mhaidra[13], Patrick Stowell[2], Holger Tietze-Jaensch[4], Lee Thompson[2], Jaap Velthuis[1], Michael Weekes[2]

[1] School of Physics, University of Bristol, UK
[2] Department of Physics and Astronomy, University of Sheffield, UK
[3] Warsaw University of Technology, Poland
[4] Forschungszentrum Jülich, Germany
* anna.kopp@bristol.ac.uk

***Abstract*—Methods for the non-destructive assay of nuclear waste drums are of great importance to the nuclear waste management community, especially where loss in continuity of knowledge about the content of drums happened or chemical processes altering the contents of the drums may occur. Muon scattering tomography has been shown to be a promising technique for the non-destructive assay of nuclear waste drums in a safe way. By measuring tracks of muons entering and leaving the probed sample and extracting scattering angles from the tracks, it is possible to draw conclusions about the contents of the sample and its spatial arrangement. Within the CHANCE project, a newly built large-scale mobile detector system for scanning and imaging the contents of nuclear waste drums using atmospheric muons is currently undergoing commissioning.**

I. Introduction

Non-destructive methods to assay nuclear waste drums are of great interest to the nuclear waste management community. It has been observed that chemical processes like oxidation of metals may occur within drums, possibly leading to the formation of gas bubbles or cracks. Furthermore, knowledge about the contents of legacy waste drums is not always preserved. Muon scattering tomography (MST) is a promising technique to address these problems. It allows to scan and image nuclear waste drums in a safe, non-destructive way using natural background radiation. Compared to other methods like X-ray or gamma-ray scanning it does not introduce additional artificial radiation or any additional hazards to personnel or equipment. Fitting the tracks of muons entering and leaving the probed sample allows to reconstruct approximated scattering vertices and to e.g. differentiate between various materials.

II. Muon Scattering Tomography

Muon scattering tomography uses secondary cosmic radiation to probe volumes from a safe distance. Compared to other scanning methods using e.g. X-rays or gamma rays it does not rely on a radiation source but uses atmospheric muons, particles resulting from primary cosmic radiation. These are ubiquitous and abundant at a rate of about $10\,000\,/(\mathrm{m}^2\mathrm{minute})$ at sea level, spread over a wide range of momenta and incidence angles. Muons are highly penetrating particles; it is almost impossible to stop them and they are thus ideally suited for scanning nuclear waste drums, where the nuclear waste is often embedded in concrete.

As charged particles, they undergo multiple Coulomb scattering processes when traversing matter. The projected scattering angle distribution depends on the atomic number Z of the traversed material and can be approximated as a Gaussian distribution [1] with mean zero and a standard deviation σ_μ of

$$\sigma_\mu \approx \frac{13.6\,\mathrm{MeV}}{pc\beta}\sqrt{X/X_0}\left(1 + 0.038\ln(X/X_0)\right), \qquad (1)$$

where p is the muon's momentum, βc its velocity, X the thickness of the scattering material and X_0 the material-specific radiation [2] length given by

$$X_0 \approx \frac{A \cdot 716.4\,\mathrm{g/cm}^2}{Z(Z+1)\ln(287/\sqrt{Z})}. \qquad (2)$$

Here, A is the atomic weight given in g/mol. As can be seen from equations 1 and 2, the width of the projected scattering angle distribution varies approimately with Z, making the technique particularly sensitive to materials with high atomic numbers.

Thus scattering angles from muons scattering off materials with large atomic numbers Z are more likely to be large than those from scatters in low-Z materials.

By placing multiple detector planes above and below the probed sample and measuring where the muons hit these, the trajectories of the incoming and outgoing muons are reconstructed and fitted. A scattering vertex is then reconstructed where these two trajectories meet. The assumption here that for each muon all scattering processes happen in the same location, the vertex, is not strictly correct but has been shown to be a good approximation. Scattering angles for all muons are derived from their fitted tracks.

Then, the volume under investigation is divided into voxels as described in ref. [4]. In each voxel with at least N

EPJ Web of Conferences **225**, 06008 (2020) https://doi.org/10.1051/epjconf/202022506008
ANIMMA 2019

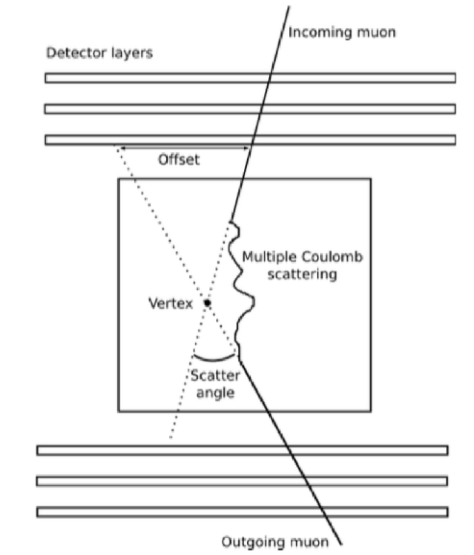

Fig. 1. Illustration of the muon trajectory and the reconstructed scattering vertex [3].

reconstructed vertices, a metric discriminator m_{ij} is calculated for each pair of tracks i and j of the N most scattered tracks,

$$m_{ij} = \frac{||\vec{v}_i - \vec{v}_j||}{(\theta_i p_i)(\theta_j p_j)}. \qquad (3)$$

Here, $\vec{v}_i$ is the location of the vertex pertaining to muon track i with momentum p_i and θ_i is the associated scattering angle. The median of this weighted metric distribution per voxel is an indicator of the predominant material in that voxel: large values are more likely to result from materials with high Z than from materials with low Z.
In the past, this has been exploited for various discrimination and identification studies in simulation: to differentiate between different high-Z materials [3], [5] or to locate gas bubbles in bitumen-filled drums [6].

III. The CHANCE Project

The CHANCE project ("Characterization of conditioned nuclear waste for its safe disposal in Europe", http://www.chance-h2020.eu), is funded by the EU's Horizon2020 research programme. It started on June 1st 2017, runs over 4 years and has 11 partners in 7 countries. Collaborators include universities and research institutes as well as government agencies and industrial partners. Within the project, three different techniques to assay nuclear waste drums in non-destructive ways are investigated: calorimetry, muon scattering tomography and cavity ring-down spectroscopy.

IV. Muon Scattering Tomography within the CHANCE Project

Three universities mainly contribute to the MST program within CHANCE: University of Sheffield, University of Bristol, both in the UK and Warsaw University of Technology, Poland. A large, mobile muon scattering tomography detector shown in figure 2 has been recently built in a non-laboratory environment outside of Bristol, UK. It is placed in a building, so it is rain-protected but the building is neither temperature- nor humidity-controlled. Thus the environmental conditions are the same as they are likely to be in an actual field deployment. The active area measures approximately $1.8 \times 1.8\,m^2$. As the detector system is modular, it is easy to dis- and reassemble and even to change the configuration to adapt it to the requirements in a potential deployment.
The detector system combines two different kinds of gas detectors, namely drift chambers and resistive plate chambers (RPCs). A coincidence between two layers of plastic scintillators is used as trigger to start the read-out process.
The RPCs were designed and built at Univeristy of Bristol. A smaller prototype of these chambers has been operated on a mixture of freon (R134-a) and isobutane in the past. Due to recent legislation restricting the usage of freon, the chambers are currently run on CO_2. Other, environmentally friendly gas mixtures will be tested in the future. The drift chambers are operated on a mix of methane, argon and CO_2. They were built at University of Sheffield.
During the construction of the detector system the data analysis effort had been focussed on simulation studies. The detector layout was optimized and a figure of merit was developed for comparing the smallest observable separations between features or the smallest observable features in concrete-filled waste drums using different reconstruction algorithms [7]. The latter is especially relevant considering the heterogeneity of real nuclear waste drums. Commissioning of the full detector system has started in early June and is ongoing, with first test data having been taken. Full data taking is expected to start soon while further simulation studies are continuing in parallel.

The Detector System

Both RPCs and drift chambers provide information in 3D space about where a muon hit the detector. As the muon traverses a detector chamber, the gas inside it gets ionized. With a high voltage applied between the top and bottom side for the RPCs or the anode wire and cathode for the drift chambers, respectively, this creates a signal, which is read out and digitized. The spatial resolution of the RPCs is in the sub-millimeter range [8], while that of the drift chambers is in the order of mm. The time resolution for RPCs with a 2mm gap as the ones used here is on the order of nanoseconds.
In both the detector stack above and below the sample space, two space points from the RPCs and three from the drift chambers are measured and read out. Hence it is possible to fit tracks and extract scattering angles with high precision. The detectors are fast, with data acquisition per event taking

2

EPJ Web of Conferences **225**, 06008 (2020) https://doi.org/10.1051/epjconf/202022506008
ANIMMA 2019

Fig. 2. The muon scattering tomography detector system of the CHANCE project. Shown are the detector systems above and below the empty sample space consisting of three layers of drift chambers and two RPC layers. The top stack additionally contains two layers of plastic scintillators used as triggers. The detectors cover an area of approximately $1.8 \times 1.8\,m^2$.

on the order of a few $10\,\mu s$ and have a low cost per unit area, making them ideal for large-scale detectors. For both the RPCs and drift chambers, three individual detectors with widths of 58 and 60 cm, respectively, are placed next to each other to cover the whole active area. The support structure holding the individual chambers can be seen as empty space in the data as shown for one layer of RPCs in figure 3. Since the footprint of the active area is larger than the drums that will be scanned, it is nonetheless possible to scan whole drums and avoid dead areas by moving the drum to different locations within the sample space.

V. Conclusions and Outlook

Muon scattering tomography is a non-destructive technology well suited to investigate the contents of nuclear waste drums in a safe way, without introducing any additional radiation to the samples or personnel. A large, mobile MST detector has been built in a non-laboratory environment close to Bristol, UK, within the CHANCE project and first test data have been taken. Once the detector system is fully commissioned, full data taking will commence.
As the scattering behavior of atmospheric muons in many materials is well known from simulation studies, data with blocks of high-Z materials like lead or tungsten will be taken in a first step. Subsequently, 'blind tests' with drums mimicking nuclear waste drums will be carried out. Our collaboration partners at SCK-CEN, Belgium, filled drums

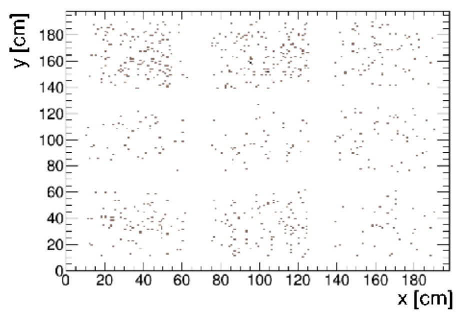

Fig. 3. Hits in one layer of RPCs. The pattern is due to the support structure holding the individual detector chambers. Each entry corresponds to one hit, showing the *x* and *y* coordinates.

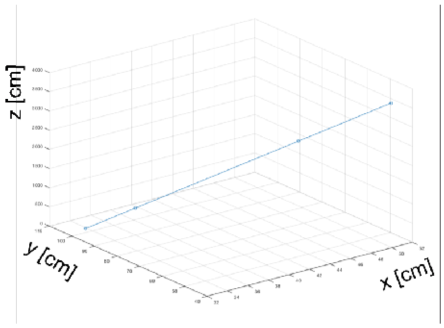

Fig. 4. Muon track fitted through all four layers of RPCs. No sample is placed between the upper and lower detectors so no scattering is expected or seen.

with non-radioactive materials otherwise similar to what could be found in nuclear waste drums but did not reveal the contents. Scanning the drums and applying the reconstruction algorithm described above will then show their contents. The access and application to real waste drums is currently being investigated.

Acknowledgment

This project has received funding from the European Union's Horizon2020 research and innovation programme under grant agreement number 755371.

References

[1] M. Tanabashi et al., "Review of particle physics," *Phys. Rev. D*, vol. 98, p. 030001, Aug 2018. [Online]. Available: https://link.aps.org/doi/10.1103/PhysRevD.98.030001
[2] T. A. Lasinsky et al., "Review of particle properties particle data group," *Rev. Mod. Phys.*, vol. 45, pp. S1–S175, Apr 1973. [Online]. Available: https://link.aps.org/doi/10.1103/RevModPhys.45.S1

EPJ Web of Conferences **225**, 06008 (2020) https://doi.org/10.1051/epjconf/202022506008
ANIMMA 2019

[3] L. Frazão, J. Velthuis, C. Thomay, and C. Steer, "Discrimination of high-z materials in concrete-filled containers using muon scattering tomography," *Journal of Instrumentation*, vol. 11, no. 07, pp. P07 020–P07 020, Jul 2016. [Online]. Available: https://doi.org/10.1088/1748-0221/11/07/p07020

[4] C. Thomay, J. J. Velthuis, P. Baesso, D. Cussans, P. A. W. Morris, C. Steer, J. Burns, S. Quillin, and M. Stapleton, "A binned clustering algorithm to detect high-z material using cosmic muons," *Journal of Instrumentation*, vol. 8, no. 10, pp. P10 013–P10 013, Oct 2013. [Online]. Available: https://doi.org/10.1088/1748-0221/8/10/P10013

[5] C. Thomay, J. Velthuis, T. Poffley, P. Baesso, D. Cussans, and L. Frazão, "Passive 3d imaging of nuclear waste containers with muon scattering tomography," *Journal of Instrumentation*, vol. 11, no. 03, pp. P03 008–P03 008, Mar 2016. [Online]. Available: https://doi.org/10.1088/1748-0221/11/03/p03008

[6] M. Dobrowolska, J. Velthuis, L. Frazão, and D. Kikoła, "A novel technique for finding gas bubbles in the nuclear waste containers using muon scattering tomography," *Journal of Instrumentation*, vol. 13, no. 05, pp. P05 015–P05 015, May 2018. [Online]. Available: https://doi.org/10.1088/1748-0221/13/05/p05015

[7] J. Stowell, J. Velthuis, H. Tietze-Jaensch, A. Kopp, A. Alrheli, M. Mhaidra, L. Thompson, and D. Kikoła, "Figures of merit for the application of muon tomography to the characterization of nuclear waste drums," *Waste Management Symposia 2019*, no. 19253, March 2019.

[8] P. Baesso, D. Cussans, C. Thomay, and J. Velthuis, "Toward a RPC-based muon tomography system for cargo containers." *Journal of Instrumentation*, vol. 9, no. 10, pp. C10 041–C10 041, Oct 2014. [Online]. Available: https://doi.org/10.1088/1748-0221/9/10/c10041